FEA modelling and environmental assessment of a thin-walled composite drive shaft

Searle, Joseph; Meng, Maozhou; Summerscales, John

Published in:
Thin-Walled Structures

DOI:
10.1016/j.tws.2022.109799

Publication date:
2022

FEA Modelling and Environmental Assessment of a Thin-walled Composite Drive Shaft

Joseph Searle, Maozhou Meng*, John Summerscales
School of Engineering, Computing and Mathematics, University of Plymouth, UK
*Corresponding author: maozhou.meng@plymouth.ac.uk

Abstract: Fibre reinforced plastics (FRP) composites have been widely used in the automotive industry with the primary focus on reduced mass. However, there are relatively few reports on their application on power transmission components, such as drive shafts. This paper explores the feasibility of replacing the traditional structural steel by light weight FRP composites in a drive shaft. Three FRP composites are considered against a steel drive shaft; basalt/epoxy, carbon/epoxy, and CNT (carbon nanotubes) reinforced carbon/epoxy composites. The mechanical performance was analysed by finite element analysis (FEA) tool and classical laminate theory (CLT), while the environmental performance was evaluated by life cycle assessment (LCA) method. The study shows that with careful design a composite drive shaft can outperform the mechanical performance of a steel shaft (up to 90% mass saving, and 50% higher Factor of Safety). The study found steel shafts were preferable to FRP shafts based on embodied energy (steel total embodied energy 150MJ, FRP +325MJ). Reductions in carbon footprint from reduced emissions due to weight savings meant a carbon/epoxy shaft was preferable to a steel shaft. Two new material indices were suggested which can be used to select materials based on minimum embodied energy and global warming potential.

Keywords: Composite drive shaft, finite element analysis, classical laminate theory, environmental impact, life cycle assessment (LCA)

Nomenclature

ACP	advanced composite prepost	J	polar moment of inertia
B/BE	basalt/bio-epoxy	κ	curvature vector
C/CNT/ E	carbon/carbon-nanotube/epoxy	LCA	life cycle assessment
C/E	carbon/epoxy	L_{cnt}	length of CNT
CER	cost estimation relations	m	mass per unit length
CF	carbon fibre	M	moment per unit vector
CLT	classic laminate theory	N	force per unit vector
CNT	carbon nanotubes	NF	natural fibre
d_{cnt}	diameter of CNT	PROMA L	program for micromechanical and micromechanical analysis of laminates
DMM	decision matrix method	Q_{11}	Reduced stiffness matrix in local coordinate system
$E_1\ E_2\ E_3$	composite principal elastic moduli	$\overline{Q_{11}}$	Reduced stiffness matrix in global coordinate system
E_{cnt}	elastic modulus of CNT	r	inner radius
E_f	fibre axial elastic modulus	R	outer radius
E_{2f}	fibre transverse elastic modulus	r_{cnt}	radius CNT
E_m	elastic modulus of matrix	RIFT	resin infusion under flexible tooling
E_{m-cnt}	effective elastic modulus CNT infused matrix	r_m	mean radius
$E_x\ E_y$	material elastic modulus in axial and hoop direction	RTM	resin transfer moulding
$F_1\ F_2\ F_3$ $F_{11}F_{12}$	Tsai-Wu parameters	T	torque
FEA	finite element analysis	t	laminate thickness
FoS	factor of safety	T_c	critical torsional buckling torque
FRP	fibre reinforced plastics	t_{cnt}	thickness CNT
G_f	fibre shear modulus	V_{cnt}	CNT volume fraction
G_m	matrix shear modulus	v_f	fibre Poisson's ratio
G_{m-cnt}	effective shear modulus CNT infused matrix	V_f	fibre volume fraction
HLU	hand layup	v_m	matrix Poisson's ratio
I	shaft second moment of area	V_m	matrix volume fraction
IF	indicator of failure	v_{m-cnt}	effective Poisson's ratio CNT infused matrix
I_{MFA}	Puck matrix dominated tensile failure mode	Z_i	z coordinate of ply
I_{MFB}	Puck matrix dominated shear failure mode	τ_{max}	maximum shear stress
I_{MFC}	Puck matrix dominated compression failure mode	ρ	density
		$\sigma_1\ \sigma_2\ \sigma_3$ $\sigma_{11}\sigma_{12}$	Stresses in local coordinate system

1 Introduction

Drive shafts are used in many applications for torque and power transmission from engine to the differential gears such as in automobiles, pumping, boats, generators, etc. Fig.1 shows an illustration of a drive shaft in a road vehicle, in which terminal B connects to the engine and terminal A connects to a differential joint to turn the wheels. To transfer power a drive shaft must meet three criteria: torque transmission capability, buckling torque capability and bending natural frequency [1]. The torque transmission capability of a solid drive shaft in isotropic materials is mainly based on the materials maximum shear stress. However, a hollow section is more common to reduce total weight so torsional buckling must be considered in the design phase.

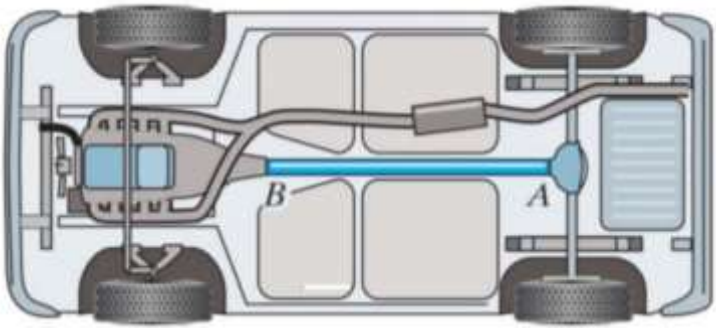

Figure 1 Illustration of a drive shaft in a vehicle [2].

Drive shafts are typically made from metals such as steel [2]. Metal drive shafts are limited by their weight and low critical speed [1]. As metals have low specific stiffness, the length of metal drive shafts is limited [3]. Composite materials are generally used due to their high stiffness and low weight. Each reduction of 10% in the mass of a vehicle would reduce fuel consumption by 6-8%, depending on the type of vehicle [4]. The research and commercialisation of composite drive shafts can be traced back to Renault vehicles, offering many benefits, including, a) up to 80% mass saving comparing to steel drive shaft; b) easy to achieve design specification like weight, strength, power consumption with careful lay-up strategy; c) easy to achieve a higher natural bending frequency than steel drive shafts and d) can be used in extreme vibration conditions [5].

The design specification of a drive shaft seeks to minimise three performance criteria: factor of safety (stress based), buckling torque and natural frequency. Due to the differing constituents in composite materials their failure modes differ from homogenous materials, therefore, composite specific failure modes must be used to calculate the factor of safety (FoS). As composite materials are normally orthotropic, drive shaft performance is strongly dependent on the chosen lay-up. Composite manufacturing processes must also be considered in the design stage. The chosen manufacturing process can affect the final composite mechanical properties, cost, and environmental impact.

The design considerations of various researchers are summarised in Table 1. Most researchers calculate stress in the driveshaft using the von Mises failure criterion. The von Mises (VM) failure criterion is "inherently isotropic, and therefore may yield incorrect results for anisotropic [materials]"[6]. The VM failure criterion is "a good option for ductile materials with equal tensile and compressive strength, but it fails with brittle materials" [7], so care must be exercised in interpreting composite failure with VM.

Table 1 A summary of current publications on composite drive shaft.

Literature	Performance Criteria Considered			Composite Properties Calculation	Additional Factors Considered
	FoS	Buckling Torque	Natural Frequency		
[8]	von-Mises Stress	Yes	No	ANSYS	None
[9]	Unclear	Yes	Yes	ANSYS	None
[10]	Von-Mises and Shear Stress	Yes	Yes	ANSYS	None
[11]	Tsai-Wu and Maximum Stress	Yes	Yes	PROMAL*	Cost
[12]	Classic Laminate Theory	Yes	Yes	Classic Laminate Theory	None
[13]	Shear Stress	Yes	Yes	Rule of Mixtures	None
[14]	von-Mises Stress	No	No	ANSYS	None
PROMAL (Program for Micromechanical and Macromechanical Analysis of Laminates)					

According to Hueber [15], the cost of composites are mainly analysed in 3 ways: i) estimation that assumes similar parts have similar costs, ii) parametric estimation that predicts the cost based on Cost Estimation Relations (CER), and iii) bottom-up estimation of the cost of material, infrastructure, work, etc to produce a final cost for the product. Another approach is from manufacturing point of view. Bader [16] performed a study for the manufacturing cost of a single component based on various materials and manufacturing processes, and found that expensive carbon could be more economic than cheaper glass.

Rising temperatures caused by release of greenhouse gases are linked to an increase in extreme weather events [17]. Socio-economic effects from extreme climate events can decrease national GDP [18]. Governments and businesses are having to take responsibility for their environmental impact. Assessment of the environmental impacts of a product or series of products is normally done via life cycle assessment (LCA) in accordance ISO 14040:2006. LCA follows the four steps:

- Goal and Scope Definition: Definition of a "functional unit", setting the system boundary and deciding what processes will be considered.
- Inventory Analysis: Characterising the process material and energy flows
- Impact Assessment: Calculating the impact of the process
- Interpretation: Analysing the impacts

In general, LCA may be inaccurate or can produce misleading results due to the uncertainty around the data used, incorrect system boundaries, limitations in data for individual impact categories, use of proxies and allocation of the products impact to waste streams [19]. Various authors have discussed the environmental impact of composites in automotive components, especially fuel saving over the use phase. Generally composite materials have been found to reduce the environmental impacts of automotive components. It is important to note that efficient recycling of composite is being extensively researched. La Rosa et al. compared a commercially available bio-epoxy resin with a petroleum-based epoxy resin [20], and they

found that bio-based resin has lower environmental impact than traditional materials. Witik et al. compared the impact of using steel to produce an automotive bulkhead against various composite materials and they found that composite materials offered a reduction of fuel usage over the part lifetime [21].

This paper aims to compare the steel and composite drive shafts based on performance, cost, and environmental impacts. The performance assessment includes torsional buckling, natural frequency, fatigue, and factor of safety by using classical laminate theory (CLT) and finite element analysis (FEA) methods. The cost and environmental impact assessment were based on LCA method. Composite drive shafts were able to meet or exceed the performance criteria of steel shafts, which may be useful as a guideline for automotive industry.

2 Definition of Scope

The motivation of this study was to explore the feasibility of replacing the traditional structural steel by Fibre Reinforced Plastics (FRP) composites in a drive shaft, considering mechanical, economic, and environmental performance.

The initial composite drive shaft example is taken from Kaw's textbook 'Mechanics of Composite Materials', where he proposed a composite drive shaft example to demonstrate the analysis design and failure of composite laminates by using classical laminate theory [22]. The example assumes a single-piece drive shaft in a typical civil vehicle is 1480mm long, and 100mm outside diameter. Other constraints include maximum torque 550Nm, minimum bending natural frequency above 80Hz (equivalent to 4800rpm) and minimum factor of safety FoS=3.

This study extends the scope of the example by introducing FEA but not limiting the fibre orientation and undertaking LCA. Five evaluation criteria were considered in this study, including (i) factor of safety based on stress limit, (ii) critical torsional buckling load, (iii) natural frequency, and (iv) cost and (v) environmental impact. Table 2 summarises the mechanical design criteria.

Table 2 Design specification of the drive shaft.

Torque (Nm)	550
Minimum natural frequency (Hz)	80
FoS	3
Length (mm)	1480
Outside radius (mm)	50

In a rotational shaft, the maximum shear stress is given by the following formula [23].

$$\tau_{max} = \frac{TR}{J} \tag{1}$$

where τ_{max} is maximum shear stress, T is the applied torque, r is the inner radius, R is outer radius, and J is polar moment of inertia $J = \pi \frac{R^4 - r^4}{2}$.

Equation 1 is purely based on geometry and the loading, without the material properties. To satisfy the design constraint of minimum FoS = 3, the material strength should be no less than three times this maximum shear stress. A hollow shaft may become instable (buckle) under

torsional loading if the wall thickness is too thin. Critical buckling torque for hollow shafts can be calculated by the following formula [23].

$$T_C = 2\pi {r_m}^2 t \times 0.272 \times ({E_x {E_y}^3})^{\frac{1}{4}} \times (\frac{t}{r_m})^{\frac{3}{2}} \quad (2)$$

where T_C is the critical buckling torque, r_m is the mean radius $= \frac{R-r}{2}$, t is the shaft wall thickness, E_x is the material elastic modulus in axial direction, E_y is the elastic modulus in hoop direction.

If the natural frequency of the shaft matches the frequency of a periodic load acting upon it (i.e., 4800rpm in this study), it could lead to resonance and failure. The fundamental natural frequency of a shaft is determined by many factors, such as material properties (i.e., elastic modulus, density), geometry (second moment of area) and boundary condition. If it is assumed that the drive shaft is simply supported, then the following equation can be applied to evaluate the first mode bending natural frequency [24].

$$f_n = \frac{\pi}{2}\sqrt{\frac{E_x I}{mL^4}} = \frac{\pi}{4}\sqrt{\frac{E_x(\mathrm{R}^2+\mathrm{r}^2)}{\rho L^4}} \quad (3)$$

where m is mass per unit length of the shaft $m = \pi(\mathrm{R}^2 - \mathrm{r}^2)\rho$, ρ is the density, L is the shaft length, I is the shaft second moment of area $I = \pi(\mathrm{R}^4 - \mathrm{r}^4)/4$.

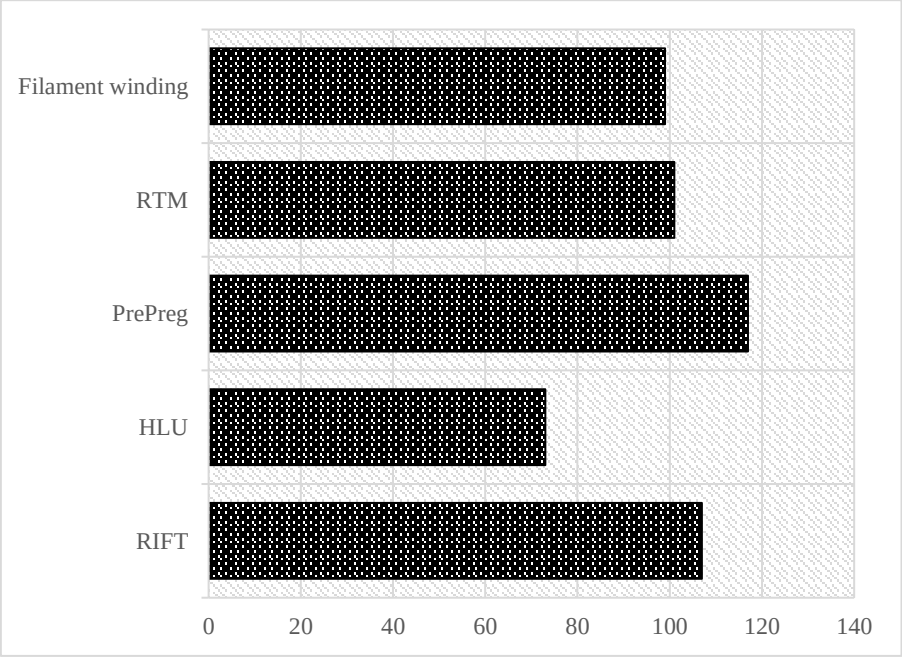

Figure 2 Manufacturing ranking from decision matrix. RTM: resin transfer moulding; HLU: hand lay-up; RIFT: resin infusion under flexible tooling. Larger score mean process is preferable.

The material selection in this study uses the principle of so-called decision matrix method (DMM), which defines criteria, weights them and appropriately sums the criteria to give a relative ranking [25]. Materials to select include synthetic/natural fibres and synthetic/bio-based matrices. The criteria to evaluate include manufacturing capacity, density, cost, stiffness, strength, embodied energy, recyclability, maximum operating temperature, renewable source, and manufacturing process [26-37]. Each criterion has a weight of 5 scores, and the materials

are ranked by the total score. Fig.2-4 show the ranking for various manufacturing process, fibres, and matrices based on the respective decision matrix. The score of each category of these materials and the relevant literature are presented in Appendix A. From Fig.2-4 the most appropriate fibres would be carbon or basalt, while the most appropriate matrices are epoxy or bio-based epoxy resin. It has been reported that small amount of carbon nanotubes (CNT), i.e., 0.5-1wt%, can increase the strength of carbon/epoxy composites by 7-16% without changing the modulus [38-40]. Based on this DMM, three composites were chosen for study, including carbon/epoxy (C/E), basalt/bio-epoxy (B/BE) and carbon/CNT/epoxy (C/CNT/E).

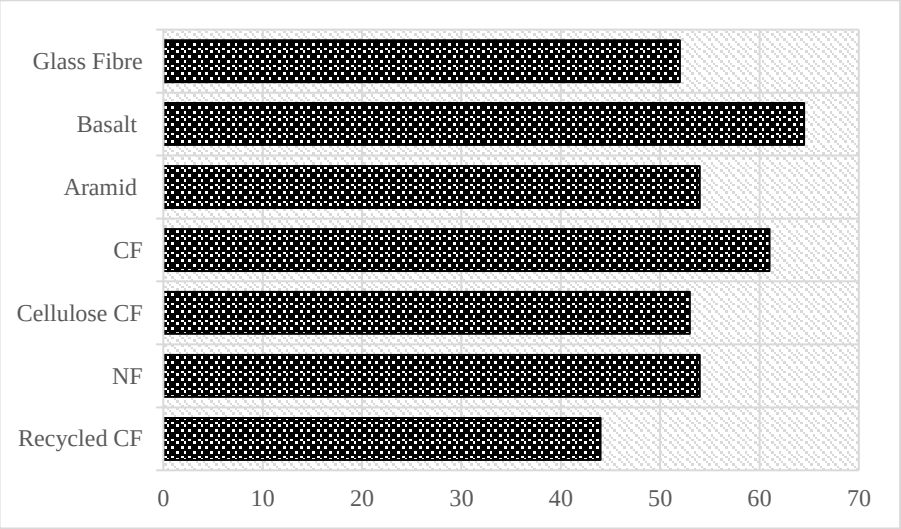

Figure 3 Fibre ranking from decision matrix.CF: carbon fibre; NF: natural fibre

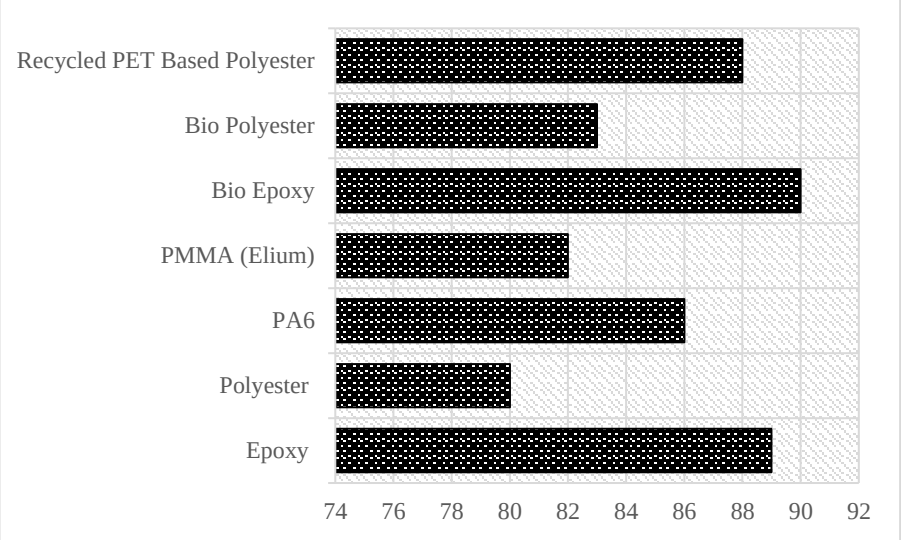

Figure 4 Fig.4. Matrix ranking from decision matrix.

The CNT volume fraction in the C/CNT/E laminate was assumed to be 0.75% in this study and the properties of matrix/CNT were calculated based on work by Dillard's [41],

$$E_{m-cnt} = \frac{3}{8}\frac{1+2\left(\frac{l_{cnt}}{d_{cnt}}\right)\beta_1 V_{cnt}}{1-\beta_1 V_{cnt}} \times E_m + \frac{5}{8}\frac{1+2\beta_2 V_{cnt}}{1-\beta_2 V_{cnt}} \times E_m \quad (4)$$

$$G_{m-cnt} = \frac{1}{8}\frac{1+2\left(\frac{l_{cnt}}{d_{cnt}}\right)\beta_1 V_{cnt}}{1-\beta_1 V_{cnt}} \times E_m + \frac{2}{8}\frac{1+2\beta_2 V_{cnt}}{1-\beta_2 V_{cnt}} \times E_m \quad (5)$$

$$v_{m-cnt} = \frac{E_{m-cnt}}{2G_{m-cnt}} - 1 \quad (6)$$

$$\beta_1 = \frac{\frac{E_{eq}}{E_m} - 1}{\frac{E_{eq}}{E_m} + 2\frac{l_{cnt}}{d_{cnt}}}, \beta_2 = \frac{\frac{E_{eq}}{E_m} - 1}{\frac{E_{eq}}{E_m} + 2}, E_{eq} = \frac{2t}{r}E_{cnt}$$

where $E_{m-cnt}, G_{m-cnt}, v_{m-cnt}$ are the effective elastic modulus, shear modulus and Poisson's ratio of matrix/CNT, $\frac{l_{cnt}}{d_{cnt}}$ is the aspect ratio of CNT, V_{cnt} is the CNT volume fraction, E_m is the elastic modulus of matrix, $t_{cnt}, r_{cnt}, E_{cnt}$ are thickness, radius and elastic modulus of CNT. The material properties of carbon fibre [42], basalt fibre [43], epoxy [42], bio-epoxy [44] and CNT [45, 46] were from literature, in which the transverse elastic modulus of carbon fibres was assumed to be 10% of longitudinal one. Fibre volume fraction was assumed to be 60% for all three composites. Mechanical properties were calculated by Equation 7-12 from Georgantzinos' article [46], and the results are presented in Table 3.

Table 3 Mechanical properties of the three types of laminae used in this study. Lamina thickness is assumed to be 0.125mm and volume fraction assumed to be 60%.

	Unit	**B/BE**	**C/E**	**C/CNT/E**	**Steel**
$\boldsymbol{E_1}$	GPa	54.9	139	140	200
$\boldsymbol{E_2 = E_3}$	GPa	8.9	6.4	8.3	
$\boldsymbol{v_{12} = v_{13}}$	ratio	0.26	0.31	0.32	0.3
$\boldsymbol{v_{23}}$	ratio	0.35	0.45	0.47	
$\boldsymbol{G_{12} = G_{13}}$	GPa	4.9	3.7	4.4	76.9
$\boldsymbol{G_{23}}$	GPa	2.2	2.4	2.8	
$\boldsymbol{S_1}$	MPa	1310	2172	2389	
$\boldsymbol{S_1^c}$	MPa	776	1448	1593	
$\boldsymbol{S_2}$	MPa	50	44	49	
$\boldsymbol{S_2^c}$	MPa	135	199	219	
$\boldsymbol{S_{12}}$	MPa	51	86	95	80
ρ	kg/m^3	2072	1490	1490	7850

$$E_1 = V_f E_f + V_m E_m \quad (7)$$

$$E_2 = E_3 = \left(\frac{V_f}{E_{2f}} + \frac{V_m}{E_m}\right)^{-1} \quad (8)$$

$$G_{12} = G_{13} = \frac{G_m\left(1+\zeta\eta_G V_f\right)}{1-\eta_G V_f} \quad (9)$$

$$\eta_G = \frac{\frac{G_f}{G_m} - 1}{\frac{G_f}{G_m} + \zeta}$$

$$G_{23} = \frac{E_2}{2(1+V_{23})} \tag{10}$$

$$\upsilon_{12} = \upsilon_{13} = \upsilon_f V_f + \upsilon_m V_m \tag{11}$$

$$\upsilon_{23} = \upsilon_{12} \frac{1-\upsilon_{21}}{1-\upsilon_{12}} \tag{12}$$

$$\upsilon_{21} = \upsilon_{12} \frac{E_2}{E_1}$$

where E_f, ${E_2}^f$ are elastic moduli of fibre in unidirectional and transverse directions, V_f, V_m are fibre and matrix volume fraction, G_f, G_m are fibre and matrix shear moduli, υ_f, υ_m are fibre and matrix Poisson's ratio, ζ is a geometric parameter in the Halpin-Tsai model [47] that is conventionally defined as 1 for circular fibre.

3 FEA and CLT models

3.1 FEA model definition

The performance of the drive shaft was evaluated by both FEA and CLT. ANSYS ACP (Advanced Composite Prepost) was employed for the FEA modelling while the CLT algorithm was implemented with VB macro in Microsoft Excel written by one of the authors (Meng). ANSYS ACP is an add-in toolbox integrated within the Workbench environment, which defines the composite layup and then implements the simulation via ANSYS Mechanical solver.

A cylindrical coordinate system was created for the drive shaft model, and the quasi-static analysis was chosen for the study. General guides on when a part should be modelled as a shell or solid part are vague but generally thickness should be small compared to other dimensions [48]. For the hollow tube, shell theory is recommended when the ratio of the radius to thickness is greater than 10 [49]. A comparison of shell and solid models indicates that they provide identical solutions due to the thin wall characteristics, therefore this study used shell element for the FEA modelling.

To simulate the real constraints of a drive shaft in a vehicle, both ends of the drive shaft were constrained in radial direction representing the bearing support. The end connected to differential joint was constrained in circumferential direction and the end connected to the engine had applied 550Nm torque about the axis of the shaft plus constraint in axial direction that prevents the rigid movement. Mesh dependency study was done by running a parametric analysis of the drive shaft with global mesh size against the three criteria: maximum shear stress, critical torsional buckling torque, and natural frequency. As shown in Fig.5-6, mesh size independence to the three criteria was quickly demonstrated in the first few iterations for the steel drive shaft model. However, the mesh dependency study on the composite model showed a different trend. Yeh and Tadjbakhsh suggested that geometric/material discontinuities in a composite model may cause an FEA singularity due to the stress concentration between interfacial layers [50]. Stress components equalise when element size is above 10mm, as shown in Fig. 5. Therefore, an element size of 10mm was chosen for the composite model, as shown in Fig.7.

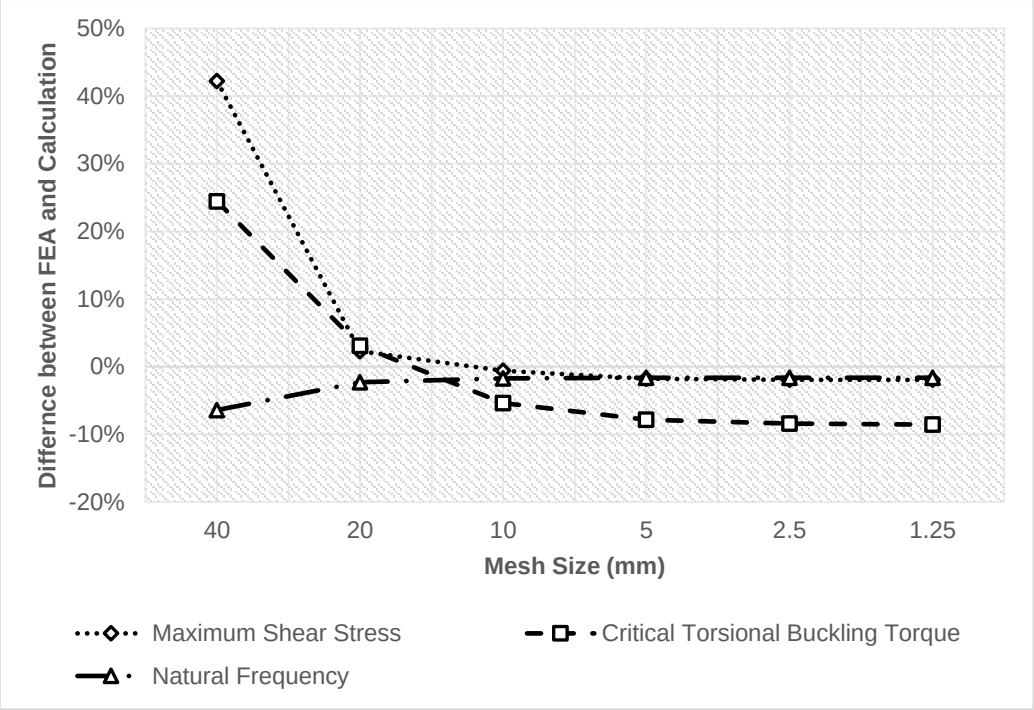

Figure 5 Mesh independency study shows a quick convergence to the criteria in the steel drive shaft.

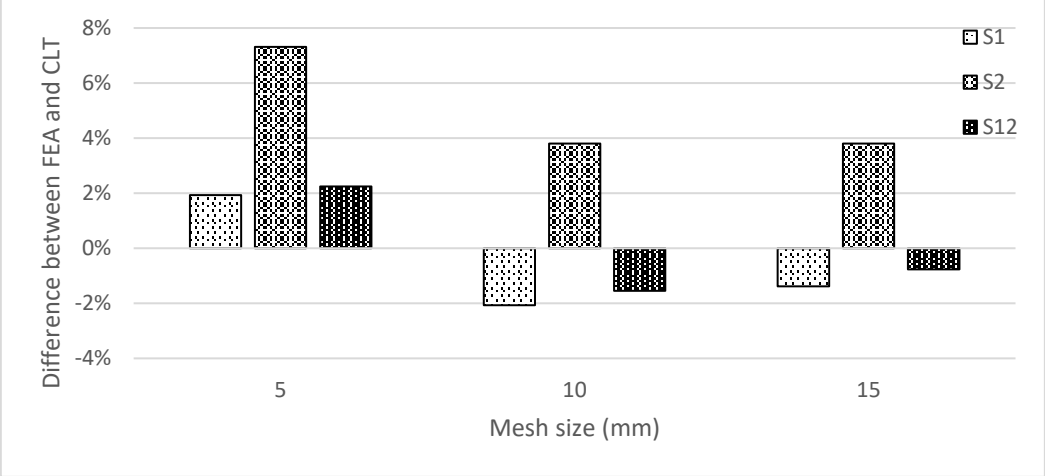

Figure 6 Effect of Mesh Size on stress components within [45] ply of the [90/±45/0/∓45/90] B/BE composite drive shaft. The chart shows the difference between FEA and CLT calculation.

Table 4 Mesh set up used in FEA model

Mesh Type	Face Sizing
Element Size (mm)	10
Behaviour	Soft
Growth rate	1.2
Capture Curvature	No
Capture Proximity	No

As composites consist of fibre and matrix phases their response to stress is dependent on the interaction between the two phases. The direction and type of stress applied affects the

composite failure mode [51]. Failure in composites either happens in the fibre, matrix, between lamina or the interfacial region between fibre and matrix. Due to these complex failure modes composite specific theories of failure have been developed. These theories can be broken down into three categories [52]: A) limit criterion – assuming failure is due to a single stress and there is no interaction between stresses; B) interactive criterion – assuming all stresses contribute to the failure of a composite; C) separate mode criterion – separating failure into fibre failure and matrix failure. Type A failure criterion limits their applications in a simple layup sequence and loading condition while Type B failure criterion over emphasises the interaction transverse fibre and matrix damage modes [53]. The World-wide Failure Exercise (WWFE) evaluated failure theories against experimental data [54], and recommended the Puck failure criterion (Type C failure criterion) for the prediction of initial/final strength and deformation of multidirectional laminates, as shown in Table 5. This study evaluated the failure mechanisms by Tsai-Wu and Puck failure criteria due to the complex layup and pure shear loading in the drive shaft.

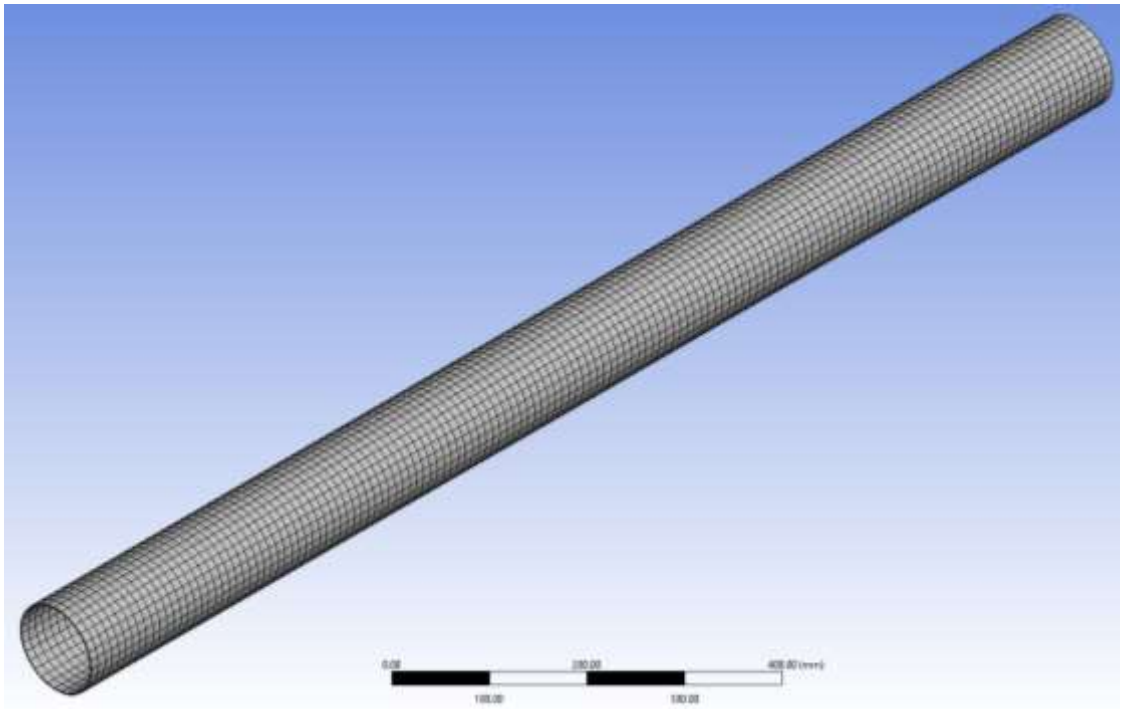

Figure 7 Mesh used in FEA model

Table 5 Failure theories for composite materials

Theory use	Recommended theory
Predicting the response of lamina	Tsai-Wu and Puck
Predicting initial strength of multidirectional laminates	Puck, Zinoviev and Wolfe-B
Predicting the final strength of multidirectional laminates	Puck, Zinoviev, Tsai-Wu or Hart-Smith.
Predicting the deformation of laminates	Zinoviev and Puck

The Puck failure criterion distinguishes between fibre failure (FF) and matrix failure (I_{MFx}), calculated based on three modes [55, 56]: Mode A - matrix dominated tensile failure, Mode B - matrix dominated shear, Mode C - matrix dominated compression (Equations 13-15).

$$I_{MFA} = ((\frac{\sigma_6}{F_6})^2 + (1 + 0.3\frac{F_2}{F_6})^2(\frac{\sigma_2}{F_2})^2)^{0.5} + 0.3\frac{\sigma_6}{F_6} \quad (13)$$

$$I_{MFB} = \frac{1}{F_6}\left(\sqrt{{\sigma_6}^2 + (0.2\sigma_2)^2} + 0.2\sigma_2\right) if \begin{cases} \sigma_2 < 0 \\ \frac{\sigma_2}{\sigma_6} \leq \frac{F_{2a}}{F_{6a}} \end{cases} \quad (14)$$

$$I_{MFC} = -\frac{F_{2c}}{\sigma_2}\left((\frac{\sigma_6}{2(1+F_{2c})F_6})^2 + (\frac{\sigma_2}{F_{2c}})^2\right) if \begin{cases} \sigma_2 < 0 \\ \frac{\sigma_2}{\sigma_6} \geq \frac{F_{2a}}{F_{6a}} \end{cases} \quad (15)$$

$$FF = \begin{cases} \frac{\sigma_1}{{\sigma_{1t}}^*} \; if \; \sigma_1 > 0 \\ \frac{-\sigma_1}{{\sigma_{1c}}^*} \; if \; \sigma_1 < 0 \end{cases}$$

$$F_{2a} = \frac{F_6}{0.4}(\sqrt{1 + 0.4\frac{F_{2c}}{F_6}} - 1)$$

$$F_{6a} = F_6\sqrt{1 + 2p_{6c}}$$

$$p_{2c} = \frac{F_{2a}}{F_6}$$

$$\begin{bmatrix} \sigma_{11} & \sigma_{12} & \sigma_{13} \\ \sigma_{12} & \sigma_{22} & \sigma_{23} \\ \sigma_{13} & \sigma_{23} & \sigma_{33} \end{bmatrix} = \begin{bmatrix} \sigma_1 & \sigma_6 & \sigma_5 \\ \sigma_6 & \sigma_2 & \sigma_4 \\ \sigma_5 & \sigma_4 & \sigma_3 \end{bmatrix}$$

Where I_{MFA}, I_{MFB} and I_{MFC} are the matrix dominated failure mode and FF is the fibre failure mode. P_{6t} and P_{6c} are fitting terms assumed to be 0.3-0.35 and 0.2-0.25. ANSYS ACP uses respective value of 0.35 and 0.25 for carbon fibre. The FoS from Puck criterion is estimated as $FoS = \min(\frac{1}{I_{MFA}}, \frac{1}{I_{MFB}}, \frac{1}{I_{MFC}})$.

The Tsai-Wu failure criterion is a generalisation of the tensor failure criterion that is an extension of Tsai-Hill failure criterion by introducing the compressive strength of composite materials. Tsai-Wu failure criterion can be written in either stress space or strain space [57], and in this study, it is mainly considered in stress space in plane stress state [58],

$$F_{ij}\sigma_i\sigma_j + F_i\sigma_i = IF \quad (16)$$

$$F_{11} = \frac{1}{S_1S_1^c}, F_{22} = \frac{1}{S_2S_2^c}, F_{66} = \frac{1}{S^2}, F_{12} = -\frac{1}{2}\sqrt{\frac{1}{S_1S_1^cS_2S_2^c}} \; F_1 = \frac{1}{S_1} - \frac{1}{S_1^c}, F_2 = \frac{1}{S_2} - \frac{1}{S_2^c}$$

where F_i and F_{ij} are strength parameters in stress space, S_1 and S_1^c are longitudinal tensile and compressive strength, S_2 and S_2^c are transverse tensile and compressive strength, S is the shear strength. IF is the indicator of failure – composite is considered to fail if IF≥1. The factor of safety (FoS) from Tsai-Wu failure criterion can be evaluated by linearly scaling up each stress component in Equation 16,

$$F_{ij}(FoS)\sigma_i(FoS)\sigma_j + F_i(FoS)\sigma_i = 1 \quad (17)$$

$$(F_{11}\sigma_1^2 + F_{22}\sigma_2^2 + F_{66}\tau_{12}^2 - F_{11}\sigma_1\sigma_2)(FoS)^2 + (F_1\sigma_1 + F_2\sigma_2)(FoS) = 1$$

Solving this quadratic equation yields

$$FoS = \frac{1}{2A}\left(\sqrt{B^2 + 4A} - B\right) \tag{18}$$

$$A = F_{11}\sigma_1^2 + F_{22}\sigma_2^2 + F_{66}\tau_{12}^2 - F_{11}\sigma_1\sigma_2$$

$$B = F_1\sigma_1 + F_2\sigma_2$$

If tensile and compressive strength are the same (or similar), the term B approximates to zero while the term A dominates Equation 18, and then the factor of safety can be simplified as

$$FoS = 1/\sqrt{IF} \tag{19}$$

3.2 CLT model definition

The CLT model evolved from works in 1950s - 60s by several researchers [59-62], CLT assumes the composite laminate is a thin-wall structure (shell) and forms the stress-strain transformation for individual orthotropic lamina. In the past few decades, numerous researches have proven that CLT model provides accurate mechanical properties and predicts consistent mechanical behaviour of composite laminate when the laminates is classified as thin-wall so that edge-effects are eliminated. The FEA simulation was validated by CLT calculation in this work, and the initial composite stacking sequence was also developed based on CLT calculation.

The fundamental assumption of CLT model is that the stress stage is simplified into 2D plane stress, therefore the 6x6 stiffness matrix is reduced to be a 3x3 reduced stiffness matrix $\bar{Q}$ [63],

$$\begin{bmatrix}\sigma_x \\ \sigma_y \\ \tau_{xy}\end{bmatrix} = \begin{bmatrix}\overline{Q_{11}} & \overline{Q_{12}} & \overline{Q_{16}} \\ \overline{Q_{12}} & \overline{Q_{22}} & \overline{Q_{26}} \\ \overline{Q_{16}} & \overline{Q_{26}} & \overline{Q_{66}}\end{bmatrix}\begin{bmatrix}\varepsilon_x \\ \varepsilon_y \\ \gamma_{xy}\end{bmatrix} \tag{20}$$

$$Q_{11} = \frac{E_1}{1-\nu_{12}\nu_{21}}, Q_{12} = \frac{\nu_{12}E_2}{1-\nu_{12}\nu_{21}}, Q_{22} = \frac{E_2}{1-\nu_{12}\nu_{21}}, Q_{12} = G_{12}$$

$$\bar{Q}_{11} = Q_{11}\cos\theta^4 + 2(Q_{12} + 2Q_{66})\sin\theta^2\cos\theta^2 + Q_{22}\sin\theta^4$$

$$\bar{Q}_{12} = Q_{12}(\cos\theta^4 + \sin\theta^4) + (Q_{11} + Q_{22} - 4Q_{66})\sin\theta^2\cos\theta^2$$

$$\bar{Q}_{22} = Q_{11}\sin\theta^4 + 2(Q_{12} + 2Q_{66})\sin\theta^2\cos\theta^2 + Q_{22}\cos\theta^4$$

$$Q_{16} = (Q_{11} - Q_{12} - 2Q_{66})\sin\theta\cos\theta^3 + (Q_{12} - Q_{22} + 2Q_{66})\cos\theta\sin\theta^3$$

$$Q_{26} = (Q_{11} - Q_{12} - 2Q_{66})\cos\theta\sin\theta^3 + (Q_{12} - Q_{22} + 2Q_{66})\sin\theta\cos\theta^3$$

$$Q_{66} = (Q_{11} + Q_{22} - 2Q_{12} - 2Q_{66})\cos\theta^2\sin\theta^2 + Q_{66}(\sin\theta^4 + \cos\theta^4)$$

where θ is the off-axis angle of a ply. Considering a composite laminate constituted by multiple plies with various off-axis angles, a 6x6 [ABBD] matrix can be constructed to form an equilibrium equation by introducing a virtual force per unit length vector [N] and moment per unit length vector [M],

$$\begin{bmatrix}N \\ M\end{bmatrix} = \begin{bmatrix}A & B \\ B & D\end{bmatrix}\begin{bmatrix}\varepsilon \\ \kappa\end{bmatrix} \tag{21}$$

$$[A] = \sum_{K=1}^{N} (\bar{Q}_{ij})(Z_k - Z_{k-1})$$

$$[B] = \sum_{K=1}^{N} \frac{1}{2} (\bar{Q}_{ij})(Z_k^2 - Z_{k-1}^2)$$

$$[D] = \sum_{K=1}^{N} \frac{1}{3} (\bar{Q}_{ij})(Z_k^3 - Z_{k-1}^3)$$

where ε and κ are the strain and curvature vectors, $z_i$is the z coordinate of each ply about the mid-plane of the laminate. If the laminate is assumed to have a symmetric layup, then the coupling matrix [B] is zero, and then the elastic properties can be evaluated by $E_x = 1/(t * [A]_{11}^{-1})$, $E_y = 1/(t * [A]_{22}^{-1})$, where t is the total thickness of the laminate, $[A]_{11}^{-1}$ and $[A]_{22}^{-1}$ are the 11 and 22 elements of the inversion of [A] matrix respectively.

In a rotational shaft, the only non-zero loading is the torque about axis, which can be represented by N_{xy} in the CLT model,

$$\mathrm{T} = \frac{N_{xy}}{t} \pi (R^2 - r^2) r_m \tag{22}$$

where r_m is the moment arm, approximates as $r_m = \frac{R+r}{2} \approx R$. Therefore, Equation 19 can be rewritten as

$$\mathrm{T} \approx \frac{N_{xy}}{2\pi R^2} \tag{23}$$

Substituting the maximum torque 550Nm and outside radius 50mm from Table 2 into Equation 20, the shear force per unit length on the shaft can be calculated as N_{xy} =35N/mm.

Substituting $N_{xy} = 35N/mm$ into Equation 18, shear strain can be evaluated by

$$\begin{bmatrix} \varepsilon \\ \kappa \end{bmatrix} = \begin{bmatrix} A & B \\ B & D \end{bmatrix}^{-1} \begin{bmatrix} N \\ M \end{bmatrix} \tag{24}$$

And stress components can be obtained by Equation 17. It should be noted that σ_x and σ_y are non-zero due to the coupling effect even though it is pure shear loading.

4 Results and discussion

4.1 Composite layup development

As a benchmark, structural steel was used to estimate the approximate thickness of the drive shaft. Substituting the elastic modulus and shear strength of steel in Table 2 into Equation 1-3 by considering factor of safety, the wall thickness, criterial torsional buckling torque and natural frequency of steel shaft are calculated as t=1.4mm, T_c=5502Nm and f=130Hz respectively. It can be calculated that the ratio of radius to thickness of the steel shaft is approximately 36, which satisfies the criterion of shell theory. The mass of the steel shaft is calculated as 5.04kg.

From the above estimation of the steel shaft, the natural frequency is not far from the minimum requirement (130Hz vs. 80Hz), and it is mainly determined by the elastic modulus in axial direction (proportional to $\sqrt{E_x/\rho}$) according to Equation 3. Substituting the respective densities of the B/BE composite, the minimum required axial modulus $E_x$of the B/BE composite drive shaft can be calculated as 20.1GPa to achieve a minimum natural frequency of 80Hz.

For the steel shaft, the critical torsional buckling torque is far higher than the requirement (5502Nm vs. 550Nm). According to Equation 2, the critical buckling torque is mainly determined by the elastic modulus in the hoop direction and wall thickness (proportional to $\left(E_x E_y^3\right)^{1/4} t^{5/2}$). The assumption that the wall thickness of the B/BE composite shaft is the same as the steel one (which is equivalent to 11 plies where each ply is assumed as 0.125mm), then the minimum hoop modulus E_y of the B/BE composite shaft can be estimated as 19.5GPa to achieve a critical torque 550Nm. Wall thickness may be reduced if higher hoop modulus E_y is increased by placing plies in 90˚.

Table 6 Development of composite layup for B/BE composite drive shaft. At least 11 plies were required to achieve the design specification.

Lay-Up development	No. plies	E_x (GPa)	E_y (GPa)	T_c (Nm)	f_n (Hz)	FoS
$[\pm 45]_{2s}$	8	15.1	15.1	245	68	5.38
$[\pm 45_2/90/\mp 45_2]$	9	15.8	19.8	303	69	4.58
$[\pm 45_2/90_2/\mp 45_2]$	10	15.8	23.3	447	69	4.76
$[\pm 45_2/0/90/0/\mp 45_2]$	11	23.0	19.4	541	83	4.95
[±45/±55/0/90/0/∓55/∓45]	11	21.3	22.7	598	80	5.47
Requirement		20.1	19.5	550	80	3

Table 7 Composite Layup of the three composite drive shafts and their properties predicted by CLT. Comparing to the weight of the steel shaft (5.04kg), the three composite shafts showed a mass reduction of 73 % for basalt and 92% for carbon composites.

	B/BE	C/E	C/CNT/E
Layup	[±45/±55/0/90/0/∓55/∓45]	[90/±65/0/∓65/90]	[90/±65/0/∓65/90]
E_x (GPa)	21.3	27.0	27.6
E_y (GPa)	22.7	90.7	89.1
G_{xy} (GPa)	11.8	14.4	14.5
ν_{xy}	0.35	0.13	0.14
t (mm)	1.4	0.875	0.875
No. plies	11	7	7
T_c (Nm)	598	580	588
f_n (Hz)	80	107	109
FoS	5.47	5.17	5.34
Mass (kg)	1.33	0.44	0.44

As a vehicle runs both forward and backward, it is wise to design a composite drive shaft with symmetric layup. The buckling torque and natural frequency both increase with shaft thickness. As natural frequency is proportional to $\sqrt{E_x}$, plies close to 0° degrees were added. As buckling torque is proportional to $\left(E_x E_y^3\right)^{1/4}$, 90° plies were added to increase buckling torque. Neither unidirectional nor transverse plies take shear load, therefore they should be avoided unless

stiffness is insufficient for T_c and f_n. Composite layups were selected using the following steps. A layup with 8 plies of symmetric $\pm 45°$ plies of B/BE drive shaft was used as a starting point, and the number of plies was increased until both hoop and axial stiffnesses matched the minimum requirement, then some plies were adjusted to optimise the performance. Due to the relatively low stiffness, two 90° plies and one 0° ply were placed to achieve the required laminate stiffness. Table 6 presents the steps taken to determine the optimum layup for the B/BE composite shaft.

With the same procedure, the layups of C/E and C/CNT/E composite drive shafts were defined, as shown in Table 7. Due to higher unidirectional stiffness but lower density, the starting point was from 6 plies, and only 7 plies of C/E and C/CNT/E composites were needed to satisfy the requirement. As the wall of these two composite shafts is considerably thinner than the B/BE one, there is a need to boost the hoop stiffness (by placing two 90° plies outside) to meet the requirement of critical torsional buckling.

The performance of the three composite drive shafts is shown in Table 8. The steel drive shaft is also listed as a benchmark. The CLT calculation for natural frequency of the three composite drive shafts agrees very well with the FEA simulation. This is because the model has been idealised, and no pre-stress was applied. It should be noted that the value of natural frequency in Table 8 is the first non-zero frequency in Modal Analysis from ANSYS Workbench, because the drive shaft was not fully constrained so that the first two modes were 0Hz representing the rigid movement. As a contrast, the critical buckling torque showed a relatively high difference – around 5% fluctuation between CLT calculation and FEA simulation.

The B/BE shaft was made thicker than either carbon shafts to account for the low modulus of basalt fibre in comparison to carbon fibre. This increase in thickness may also explain the reduction of T_c in FEA simulation for the B/BE and steel shafts compared to the CLT calculation. The radius to thickness ratio (R/t) for the B/BE shaft was approximated to 36 while it was 57 for the carbon ones. This phenomenon was also discussed by Sadowski and Rotter [49], where the authors found that as R/t decreased, the accuracy of predicted buckling load decreased and this trend continued until a minimum R/t value of 10. The two carbon shafts showed similar performance as the embedded CNT had no obvious effects on the composite stiffness, though the presence of CNT with epoxy matrix enhanced the strength of the composite.

Table 8 A summary of composite drive shaft performance. Steel shaft is also shown for comparison. The FoS for steel shaft was based on von-Mises criterion.

		B/BE	**C/E**	**C/CNT/E**	**Steel**
$T_c(Nm)$	**CLT**	651	577	572	5273
	FEA	823	612	762	5003
	Difference (FEA/CLT)	26%	6%	33%	-5%
$f_n(Hz)$	**CLT**	93	123	127	127
	FEA	99	123	135	125
	Difference (FEA/CLT)	6%	0%	6%	-2%
FoS	**CLT (Tsai-Wu)**	5.47	5.17	5.34	3
	FEA (Puck)	4.76	6.67	6.58	3.1
	Difference (FEA/CLT)	-13%	29%	23%	3%

The steel shaft has the largest T_c and f_n due to the higher transverse modulus. However, the limitation of its shear strength constrains the potential of mass reduction for the steel shaft. Due

to the coupling effect, the loading (pure torsion in a drive shaft) can been spread to three stress components in an angle-ply composite laminate. This effect greatly improves the factor of safety of the composite drive shafts even with lower shear strength. After the stress/strain transformation between local and global coordinate systems, two non-zero elements $[A]_{16}$ and $[A]_{26}$ may appear in an angle-ply composite. These non-zero elements cause the coupling effect that induces normal/transverse stresses due to shear stress. As the unidirectional and transverse plies have no coupling effect, they are vulnerable in the pure torsion (shear) loading condition. However, to satisfy the requirement of minimum T_c and f_n, some unidirectional and transverse plies are needed in the drive shaft to boost the hoop and axial stiffnesses, as discussed in the previous section.

Shown in Fig.8-10 are the composite layups, stress components (s12 and s2) and inverse reserve failure (IRF) of Puck failure in the B/BE, C/E and C/CNT/E composite shafts respectively. The stress component s1 was not presented in the figures because it was far lower than the unidirectional strength. The three failure modes of Puck criterion (pmA, pmB and pmC) are also shown, indicating the potential failure of composite by matrix dominated tensile failure, matrix dominated shear, and matrix dominated compression. In the B/BE shaft, as shown in Fig.8 the highest value of IRF value can be found in the unidirectional 0° (pmA) and transverse 90° (pmB) plies. These plies experienced the highest shear stress (s12).

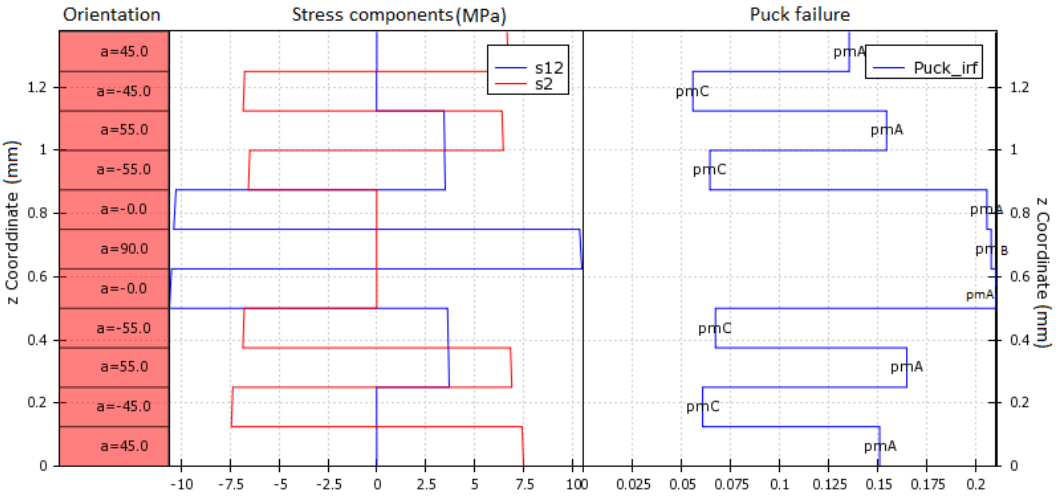

Figure 8 FEA simulation results of B/BE composite drive shaft.

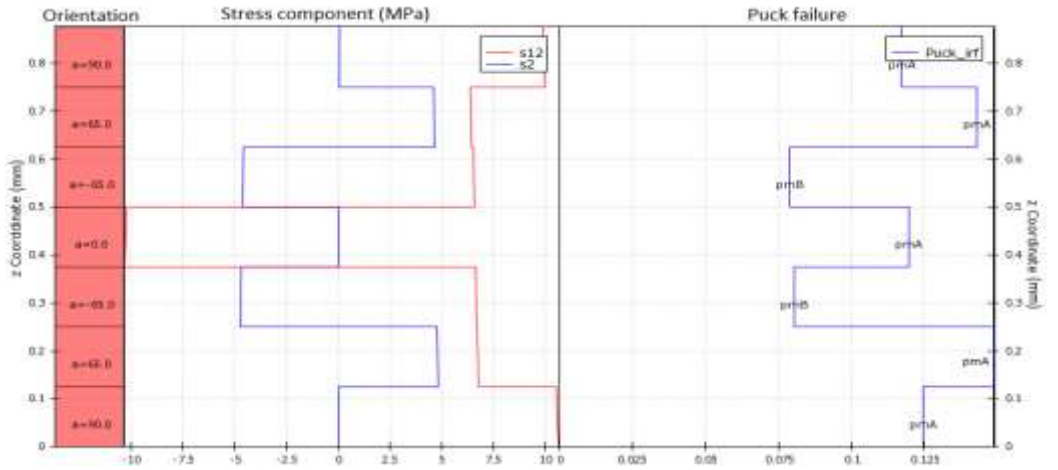

Figure 9 FEA simulation results of C/E composite drive shaft.

In the C/E and C/CNT/E shafts, the IRF value in 65° plies were even higher than either unidirectional or transverse plies. This is because the coupling effect induced transverse tensile stress that contributed significantly to the failure criterion due to relatively low transverse tensile strength. It should be noted that the predicted failure may shift to $-65°$ plies if engine works in reverse.

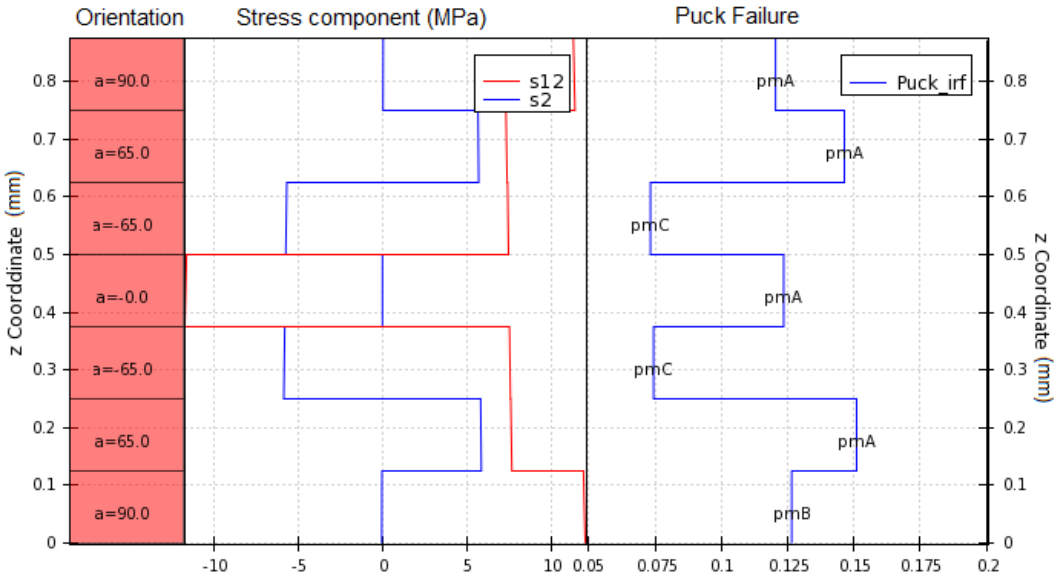

Figure 10 FEA simulation results of C/CNT/E composite drive shaft.

4.2 Fatigue estimation

There is no standard to justify the fatigue cycles from the service life of a vehicle, however it is sensible to make an assumption that the shift of a gear change counts as a fatigue cycle. A preliminary model can be developed to estimate the fatigue cycles,

$$N = \frac{2 \times V \times n_s \times n_j \times Y}{n_g} \tag{22}$$

where N is the cycle count, $V = 30MpH\ (48KpH)$ is the average speed of a journey, $n_s = 10$ is the number of stops per journey, $n_j = 261$ is the number of journeys per year, $Y = 15$ is the expected service years of the vehicle, $n_g = 10MpH(16KpH)$ is the average increment speed of a gear change. By substituting these assumptions into Equation 22, the number of cycles is estimated as $N = 3.25 \times 10^5$.

Using the fatigue data of structural steel from 1998 ASME BPV Code, Section 8, Div 2, Table 5-110.1[64], ANSYS Workbench suggested that the steel shaft had a minimum fatigue factor of safety 2.31 under the number count $N = 3.25 \times 10^5$, indicating that a steel shaft can be in service over 15 years. It should be noted that the FEA model assumed no defects in the material and loading cycles were sinusoidal. A steel shaft usually failed under low rotating-bending variable stress and fatigue crack propagated through the whole cross section of the shaft under both low-cycle and high-cycle fatigue mechanisms due to imperfection of material properties.

The estimation of fatigue life for a composite shaft is much more complicated due to the complexity of material constitution and stacking sequence. Quaresimin et al [65] recommended a simplified procedure to estimate the fatigue life of composites by defining an average fatigue

ratio φ_(50%) for 50% survivability based on experimental data at 2×10^6 cycles. Quaresimin et al [65] defined the procedure based on the concept of the fatigue ratio. Their results closely matched experimental data. The authors stated that an approximation of the S-N curve of 50% survivability can be found by simply multiplying the ultimate tensile strength by φ_(50%) and plotting a line between these points. The equation from these lines can then be used to estimate the reduction in strength. Following this approach, the S-N curves of the three composites can be drawn, as shown in Figure 11.

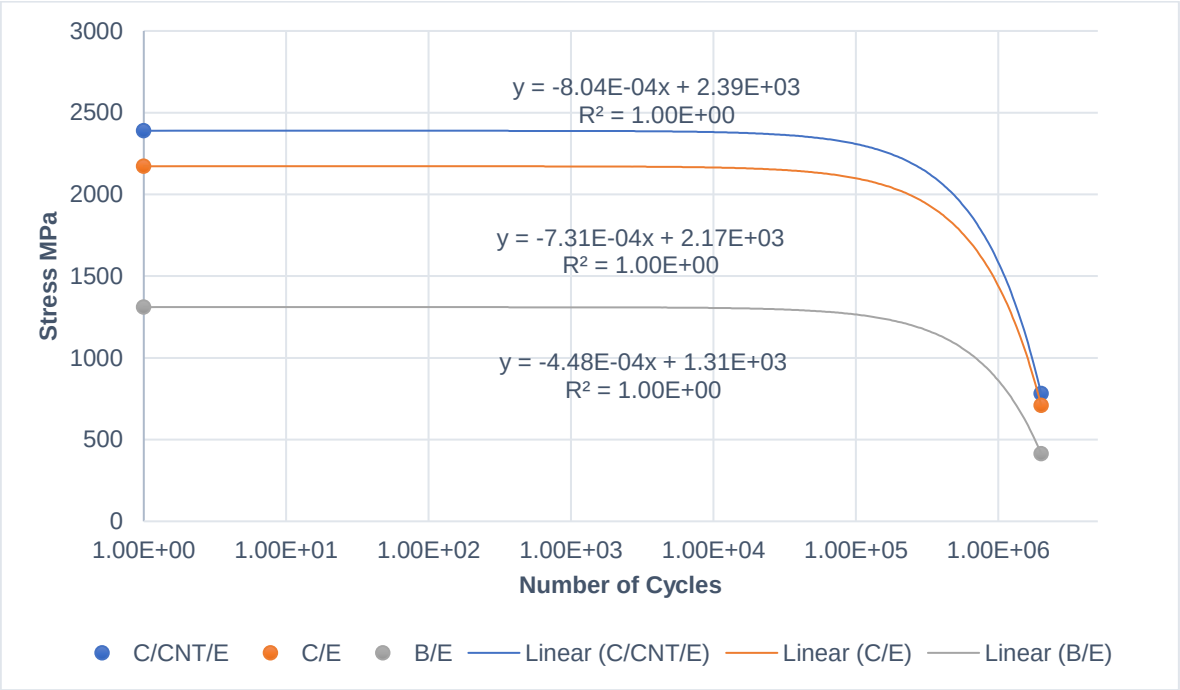

Figure 11 S-N curves of the three composites based on Quaresimin's model.

Substituting the fatigue number count $N = 3.25 \times 10^5$ into Quaresimin's model, strength reduction of the three composites (B/BE, C/E, C/CNT/E) were estimated as 11.8%, 11.3% and 10.8% respectively. Obviously, this reduction at around 11% is still way behind the failure threshold as the FoS of these composites are considerably higher than the requirement (~5-7 vs. 3).

4.3 Life Cycle Assessment

4.3.1 Goal and Scope

This life cycle assessment assessed the environmental impact and cost of a range of materials for use in an automotive driveshaft. The functional unit for the LCA was to at least match all three performance criteria of a steel drive shaft: factor of safety, natural frequency and buckling torque. The environmental impact was represented by the embodied energy (MJ) and global warming potential CO_2/kg. The assessment's scope covered the production, use and disposal of the driveshafts. The impact of materials was assessed based on mass of material.

The steel drive shaft was used as a reference case. The impact during the use phase was assessed based on mass/CO_2 savings compared to the steel shaft. The scope did not include the production of the shaft's connections assumed to be identical in all four cases. The following assumptions were made:

- For all shafts the only environmental impacts in the production stage come from material and shaft production (Mould, machinery and ancillaries excluded).
- 6 kg reduction in CO_2 for every kg saved in the component [66].
- All composite products are incinerated, in basalt composites only the resin has calorific value.

4.3.2 Inventory Analysis

Data on the impact of composite material had a large range; therefore, the maximum value, data were taken from Granta Edupack [67] where possible. The inventory and analysis were performed using Microsoft Excel, and data are shown in Table 9-10.

Table 9 Production cost and environmental impacts for each type of drive shaft

	Process	Production Cost			Production Inputs		Production Outputs	
		Shaft Mass (kg)	£/kg	Price (£)	MJ/kg	MJ	CO2 kg/kg	CO2 (kg)
Steel	Steel Production	4.9	0.7	3.6	20.5	100.5	1.6	7.6
	Total			3.6		100.5		7.6
	Process	Production Cost			Production Inputs		Production Outputs	
		Shaft Mass (kg)	£/kg	Price (£)	MJ/kg	MJ	CO2 kg/kg	CO2 (kg)
Carbon	Carbon/Epoxy Prepreg Production	0.4	32.0	13.9	750.0	326.8	50.0	21.8
	Shaft Production (Filament Winding)	0.4	5.3	2.3	2.7	1.2	1.8	0.8
	Totals			16.2		328.0		22.6
	Process	Production Cost			Production Inputs		Production Outputs	
		Shaft Mass (kg)	£/kg	Price (£)	MJ/kg	MJ	CO2 kg/kg	CO2 (kg)
Basalt	Basalt/Epoxy Prepreg Production	1.3	16.5	21.9	451.0	399.8	32.2	28.5
	Shaft Production (Filament Winding)	1.3	5.3	7.0	2.7	3.6	1.8	2.4
	Totals			29.0		403.4		31.0
	Process	Production Cost			Production Inputs		Production Outputs	
		Shaft Mass (kg)	£/kg	Price (£)	MJ/kg	MJ	CO2 kg/kg	CO2 (kg)
Nano	Carbon/Nano/Epoxy Prepreg Production	0.4	182.0	77.1	320450.0	135679.1	799.0	338.3
	Shaft Production (Filament Winding)	0.4	5.3	2.2	2.7	1.1	1.8	0.8
	Totals			79.3		135680.3		339.1

Table 10 Effect of weight savings and disposal cost and environmental impacts for each type of drive shaft

Steel	Effect of Weight Savings			Steel	Process	Shaft Mass (kg)	Disposal Cost		Disposal Inputs		Disposal Outputs	
	Weight Reduction	CO2 Saved/kg	CO2 Savings (kg)				£/kg	Cost (£)	MJ/kg	MJ	CO2 kg/kg	CO2 (kg)
	0.00	-6	0		Steel Recycling	4.90	43	210.7	8.96	43.904	0.70	3.4
			0.0			4.90		210.7		43.9		3.4

Carbon	Effect of Weight Savings			Carbon	Process	Shaft Mass (kg)	Disposal Cost		Disposal Inputs		Disposal Outputs	
	Weight Reduction	CO2 Saved/kg	CO2 Savings (kg)				£/kg	Cost (£)	MJ/kg	MJ	CO2 kg/kg	CO2 (kg)
	4.46	-6	-26.8		Carbon/Epoxy Disposal (incineration)	0.44	95	41.4	-32.9	-14.3	3.33	1.5
			-26.8			0.44		41.4		-14.3		1.5

Basalt	Effect of Weight Savings			Basalt	Process	Shaft Mass (kg)	Disposal Cost		Disposal Inputs		Disposal Outputs	
	Weight Reduction	CO2 Saved/kg	CO2 Savings (kg)				£/kg	Cost (£)	MJ/kg	MJ	CO2 kg/kg	CO2 (kg)
	3.57	-6	-21.4		Basalt/Epoxy Disposal (incineration)	1.33	95	126.3	-32.9	-43.8	3.33	4.4
			-21.4			1.33		126.3		-43.8		4.4

Nano	Effect of Weight Savings			Nano	Process	Shaft Mass (kg)	Disposal Cost		Disposal Inputs		Disposal Outputs	
	Weight Reduction	CO2 Saved/kg	CO2 Savings (kg)				£/kg	Cost (£)	MJ/kg	MJ	CO2 kg/kg	CO2 (kg)
	4.48	-6	-26.9		Carbon/Epoxy Disposal (incineration)	0.42	95	40.2	-32.9	-13.9	3.33	1.4
			-26.9			0.42		40.2		-13.9		1.4

4.3.3 Life Cycle Assessment Results

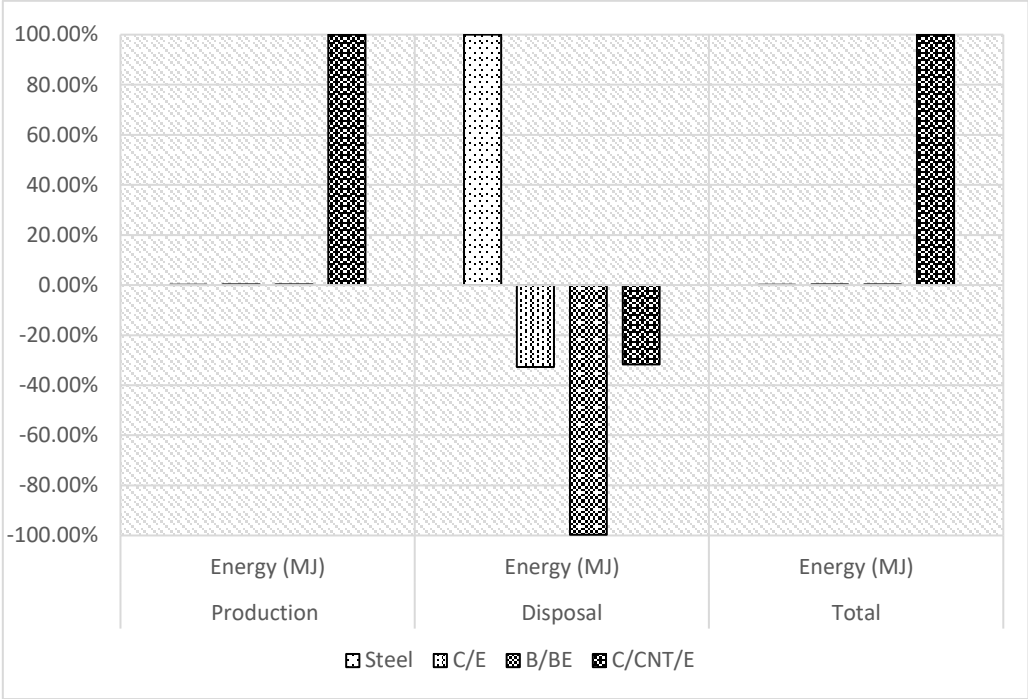

Figure 12 Normalised to maximum value, energy for the steel carbon epoxy (C/E), basalt bio-epoxy (B/BE) and carbon, carbon-nanotube, epoxy (C/CNT/E) shafts

The C/CNT/E drive shaft had the largest impact in all categories at the production stage. This is due to the high energy requirement of the chemical vapour deposition process used to produce CNT [68]. It is assumed all composite shafts are incinerated with energy recovery so have a negative embodied energy. The energy savings in the composite materials are mass based meaning the basalt shaft had the largest energy saving. Despite these savings the large production energy required in the composite shafts means their impact (EE and GWP) exceeds that of the steel shafts.

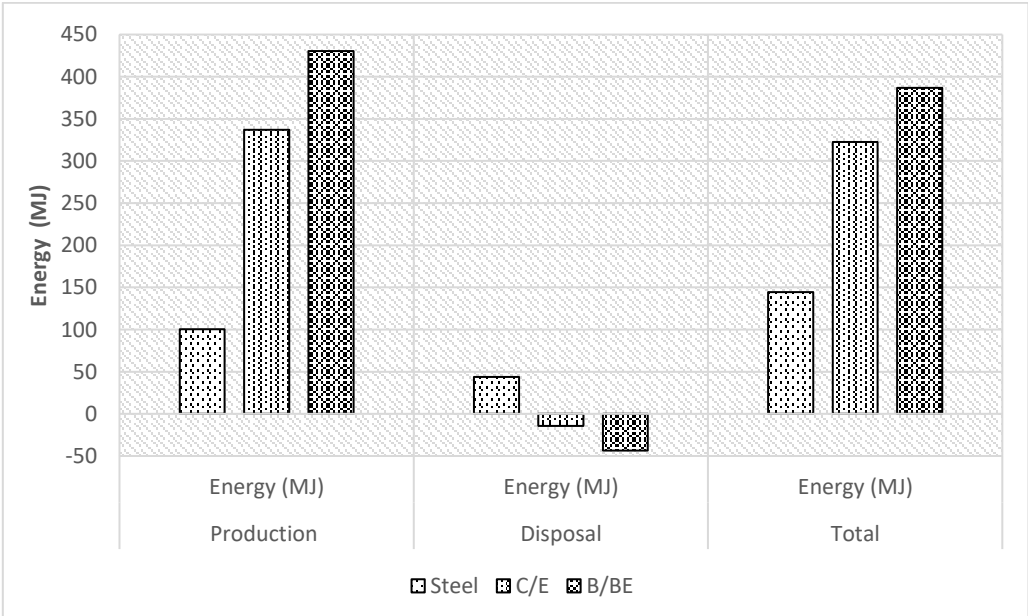

Figure 13 Energy used in the production of all drive shafts excluding the carbon, carbon-nanotube, epoxy shaft.

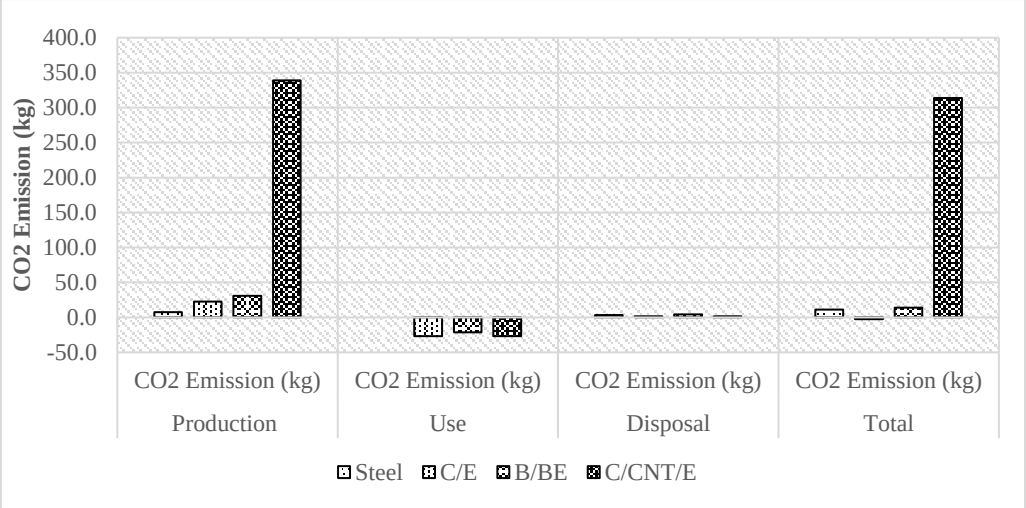

Figure 14 Lifetime CO_2 emissions for all shafts

It was assumed for every kg of weight saving there would be 6kg less CO_2 produced. As the steel shaft is used as a reference case, it has no impact in the use phases. As CO_2 saving is based on weight savings there is very little difference in the reduced CO_2 emissions in the use phase between the C/E and C/CNT/E shafts. The high energy requirements of the carbon vapour deposition production process mean the carbon footprint of the C/CNT/E shaft far exceeds that of all other shafts.

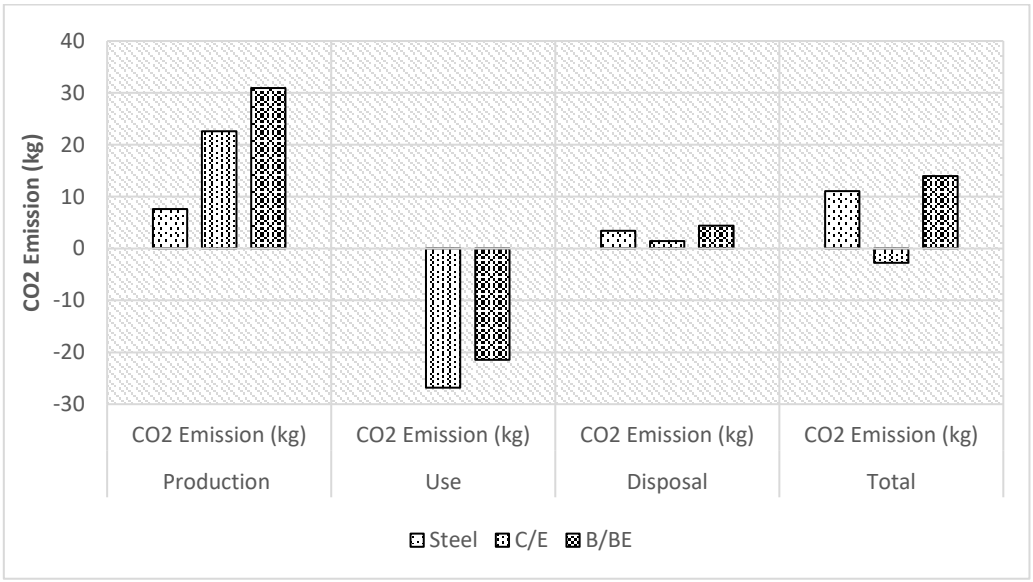

Figure 15 Lifetime CO_2 emissions excluding the C/CNT/E shaft

In the production phase the steel has significantly reduced emissions in comparison with the composite shafts. Reduced lifetime emission from weight savings means the C/E would have less impact than a steel shaft. The B/BE shaft however would produce more carbon over its lifetime. As discussed above the impact/kg of the B/BE prepreg is small in comparison to the impact of the C/E prepreg. As the material properties of the B/BE prepreg are significantly lower than properties of the C/E prepreg a larger mass is required to fulfil the same criteria. This results in the shaft having a significantly larger impact.

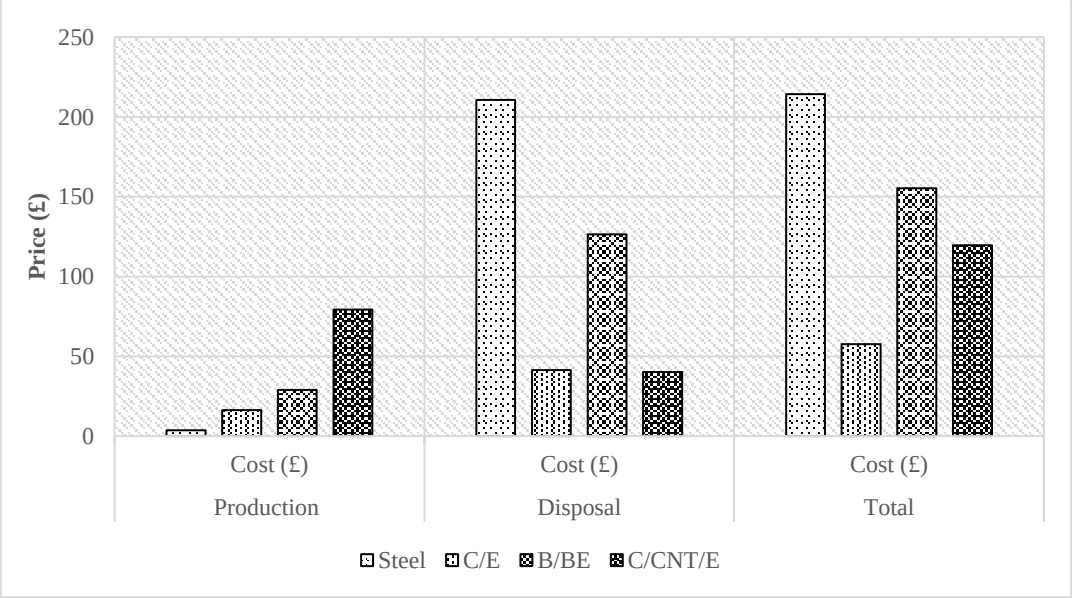

Figure 16 Estimated cost (Pounds sterling) for each shaft

In the production stage the steel drive shaft has the lowest cost. However, at the disposal stage steels recycling costs exceed all other drive shafts. This is due to the high mass of the steel shaft in comparison with the composite shafts. The carbon epoxy shaft has the lowest overall cost as it is directly proportional to mass. Basalt composite cost per kilo is approximately half that of carbon fibres (32 £/kg vs 16.5 £/kg). The basalt shaft large mass however (1.33kg vs 0.44kg) offsets the materials lower cost.

4.3.4 Interpretation of Life Cycle Assessment

The LCA showed weight savings from the use of carbon fibre/epoxy composite results in significant CO_2 savings over the parts lifetime in comparison with a steel shaft. Tatar steel assessed the lifecycle cost and CO_2 emissions of composite and steel car parts [69]. Their results showed that two unnamed composites had a higher carbon footprint over the vehicles lifetime. Tapper et. al [70] note that despite the reduced CO_2 emissions in the use phase from weight savings it is not enough to offset emissions from the production and disposal of carbon fibre products. Witik et al. compared the carbon footprint and cost of steel and glass fibre composites for use in a public footbridge. They also found that composite products had a larger carbon footprint due to the energy intensive composite production process [21].

Eberle and Franze estimated the cost and carbon footprint of steel and composite bulkheads in vehicles[71]. They found steel components had a higher cost and carbon footprint due to increased weight and fuel use. They estimated fuel use using the coefficient of reduction and in this study, it was assumed fuel savings decrease linearly with the reduction in mass.

It was assumed the only impacts from the production stage come from material production. In composite shafts this excluded the development of any moulds needed in the filament winding process. The environmental impact from the production of a mould would be shared over all shafts produced by that mould. This means any associated impact in the shaft mould production would be small and unlikely to affect results. For the steel shaft the assumption meant excluding any turning and finishing operations. Khan et al. estimated that turning consumed 20-95 MJ/mm^3 (2.5-12 MJ/kg) depending on the specific conditions [72]. The production of a steel shaft would have to consume approximately 250MJ more energy for its impact to exceed

the B/BE and C/E shafts. This would equate to an extra 2.63-12.5 m^3 (20-98 tons) of material removed depending on machining conditions.

Tapper et al. found the most efficient disposal method for composite products at end of life is incineration with energy recovery [70]. Both carbon and glass fibre composite can be burnt to recover energy, waste products from the incineration of glass fibres in a cement kiln is a common route to the production of cement [73]. Basalt fibres however do not burn and hence it was assumed only the resin produced energy when incinerated [74]. It is also assumed that the C/CNT/E composite can be disposed using incineration. Nowack, Bernd, et al. reviewed several studies covering the incineration of products containing CNT [75]. They found incineration destroyed up to 99% of CNT in parts with remain CNT existing in the slag or ash. This suggests any environmental impacts on humans/animals from the disposal of CNT will be small and can therefore be ignored.

It was observed that shaft mass, which is a function of the material mechanical properties, has a considerable effect on the overall impact of the shafts. The relationship between the material mechanical properties and ability to perform its function is well understood and Ashby's "material indices" have been suggested to aid material selection [76]. Material indices are used at the start of the design process to allow materials to be selected quickly before major design work has been completed.

The indices below are suggested for material selection for minimal environmental impact where EE is embodied energy (MJ/kg), and EC is embodied carbon (CO_2/KG). Indices shown below were stiffness prescribed as 2 out of 3 of the shaft's key parameters (natural frequency and buckling torque) were stiffness based.

$$Beam, minimum\ embodied\ energy, stiffness\ prescribed = \frac{E^{0.5}}{EE}$$

$$Beam, minimum\ carbon\ footprint, Stiffness\ prescribed = \frac{E^{0.5}}{EC}$$

Looking at material indices in Figure 17 show that steel is the preferred material. This mirrors the results from the production stage of the LCA. The material indices do not consider reduced emissions from fuel savings, this explains the difference between material indices and overall results. The material indices for the embodied energy do not reflect results observed in the LCA with a B/BE shaft being preferable to a C/E shaft. The LCA considers the impact of the shaft after layup has been set. Layups were set using CLT where the effect of both the transverse and longitudinal modulus were considered. The material indices only considered the longitudinal modulus. The material indices for carbon footprint do reflect the LCA results with C/E being shown as the preferable material. Difference in results for both indices are unlikely to be statistically different between shafts. Despite this the index may be useful design tools in the initial design process as it broadly reflects the results from production stage of the LCA.

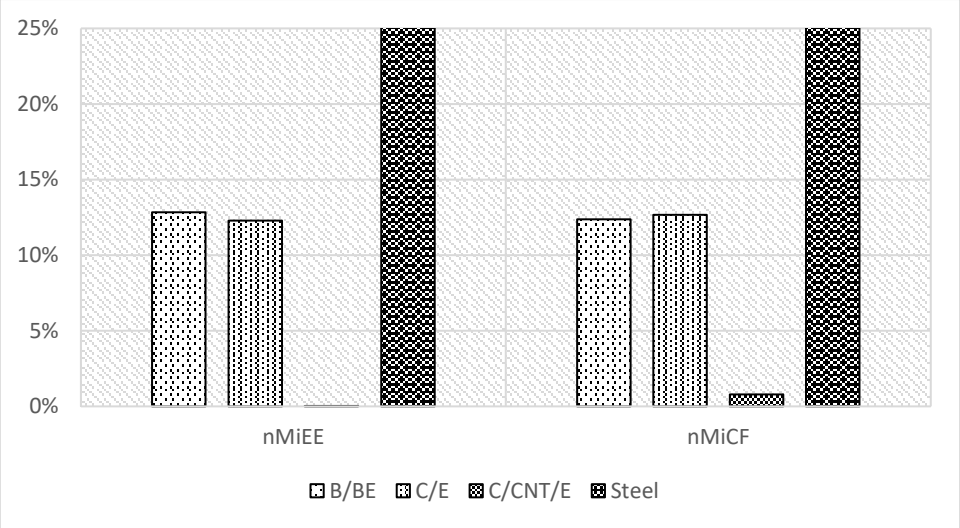

Figure 17 Normalised material indices for minimum embodied energy (nMiEE) and minimum carbon footprint (nMiCF). Longitudinal modulus and density used to calculate material indices taken from Table 3. Data from embodied energy and carbon footprint were taken from the totals row of Table 9 Note 1: material indices for C/CNT/E is less than 1% for both indices. Note 2: Axis cropped to allow data to be compared, material indices for steel is 100% in both categories.

4.4 Drive Shaft Material Selection

The most suitable composite shaft would be the either the C/E or C/CNT/E shafts in terms of performance and mass saving. Both gave a significant mass reduction (<90% of the original mass), while meeting the design requirement of the steel shaft. The B/BE shaft had the lowest natural frequency and highest reserve factor (low FoS). Additionally, the cost and embodied energy of B/BE shaft were high in comparison to the steel shaft.

The steel shaft appears to be most suitable for application where economic cost is sensitive. The composite shafts large environmental impact may limit their wide scale use due to consumer increasing concern over products environmental impacts. Steel offer clear advantages across both environmental indicators. The B/BE shaft offers a significant reduction in CO_2 but it has relatively poor material properties: a relatively large mass of material is required increasing the shafts cost and embodied energy. In applications where weight saving is crucial, such as motor racing, the C/E or C/CNT/E may be used.

5 Conclusion

This study investigates the feasibility of replacing the traditional steel by FRP composites in a vehicle drive shaft by means of classical laminate theory calculation and finite element analysis. Performance, cost, and environmental impacts were evaluated. The following conclusions were drawn from this study.

All three composites (B/BE, C/E and C/CNT/E) were able to meet the design specification by using the same or less volume of material than the steel one. The two carbon shafts even had a better mechanical performance with 35% less material usage (in volume). Considering the high specific modulus, there was a massive mass saving if replacing steel by composites (up to 90%), which benefits fuel saving thus reduces environmental impact.

Due to the coupling effects, a pure torsion/shear induced unidirectional and transverse stress, both tensile and compression in composites. A steel shaft fails under shear, at a contrast, the composite ones are more vulnerable in transverse tension. Puck failure criterion can comprehensively predict potential failure modes of composites.

Composite shafts presented a much higher factor of safety than the steel one (FoS FRP's 5.3-5.4, FOS Steel 3). This is also due to the coupling effects that spreads the pure shear to unidirectional and transverse stresses. However, care must be taken to avoid high transverse tensile stress as this is the weakest stress component in composites. Both steel and composite shafts can meet 15 years fatigue life. Considering the vibration in the real condition, the composite ones can be superior as they are well known for vibration absorption/damping.

The model used to predict the effect of carbon nanotubes on composites behaviour showed small additions of carbon nanotube had little effect on the properties of carbon/epoxy composites. Beyond this the inclusion of carbon nano tubes greatly increased the financial and environmental cost the drive shaft. Consequently, carbon nano tubes are not currently recommended for use in mass manufactured products.

Material indices were proposed for material selection in this work. These indices cannot be used to replace lifecycle assessment in the design process but may be used in initial design phase. Results from the life cycle assessment showed the carbon/epoxy shaft had a greater environmental impact than basalt bio-epoxy shaft (Steel total embodied energy 150MJ, FRP's +325MJ. This was due to the greater mass of the B/BE shaft.

The life cycle assessment showed composite only provided benefits during the use phase, due to reduced emissions from weight savings. At all other stages they have a detrimental effect on the impact of the product Reduced emissions during the use phase were not enough to offset the impact in the production/disposal stage for the B/BE and C/CNT/E shafts. The benefit is also small in the C/E shaft. This mirrors results observed by others who have studied using composite materials as a replacement for metals in automotive components.

Acknowledgement

The authors would like to acknowledge the support of the International Science and Technology Innovation Cooperation Project of Sichuan Province (2022YFH0075).

References

1. Sulthana, P.P., K. Aruna, T.K. Rao, and H. Shivakumar, *Design and analysis of drive shaft for heavy duty truck.* International Journal of Research in Engineering and Technology, 2016. **05**(01): p. 6.
2. Zaki, M.Z.M., *Design and Analysis of a Composite Drive Shaft for an Automobile*. 2012, University Malaysia Pahang.
3. El Zoghby, A., K. Maalawi, and M. Badr, *Torsional buckling optimization of composite drive shafts.* World Applied Sciences Journal, 2015. **33**(3): p. 517-524.
4. Tolouei, R. and H. Titheridge, *Vehicle mass as a determinant of fuel consumption and secondary safety performance.* Transportation research part D: transport and environment, 2009. **14**(6): p. 385-399.
5. Nadeem, S.S., G. Giridhara, and H. Rangavittal, *A Review on the design and analysis of composite drive shaft.* Materials Today: Proceedings, 2018. **5**(1): p. 2738-2741.
6. Korenczuk, C.E., L.E. Votava, R.Y. Dhume, S.B. Kizilski, G.E. Brown, R. Narain, and V.H. Barocas, *Isotropic failure criteria are not appropriate for anisotropic fibrous biological tissues.* Journal of biomechanical engineering, 2017. **139**(7).
7. Pérez-González, A., J.L. Iserte-Vilar, and C. González-Lluch, *Interpreting finite element results for brittle materials in endodontic restorations.* BioMedical Engineering OnLine, 2011. **10**(1): p. 1-16.
8. Mohanraj, R., S. Elangovan, V.K. Chandran, M.M. Sulaiman, R.H. Pradhaa, S. Poojasri, and J. Ramakrishna, *Numerical analysis on bending and contact stress of single and double start worm drive.* Materials Today: Proceedings, 2021. **46**: p. 8038-8044.
9. Shaikh, S.M., P.V. Pingale, S.G. Pinjari, P.R. Patil, T.M. Shaikh, and S.M. Godase, *Design and Analysis of Composite Drive Shaft.* Design and Analysis of Composite Drive Shaft, 2018. **05**(11): p. 1103-1107.
10. Yeswanth, I. and A.A.E. Andrews, *Parametric optimization of composite drive shaft using Ansys Workbench 14.0.* Internaltional Journal of Mechanical Engineering and Technology (IJMET), 2018. **8**(5): p. 10-23.
11. Chowdhuri, M. and R. Hossain, *Design analysis of an automotive composite drive shaft.* International Journal of Engineering and Technology, 2010. **2**(2): p. 45-48.
12. Dinesh, D. and F.A. Raju, *Optimum design and analysis of a composite drive shaft for an automobile by using genetic algorithm and ANSYS.* International Journal of Engineering Research and Applications, 2012. **2**(4): p. 1874-1880.
13. Patil, B., F. Kandagal, and M. Vinoth, *Weight optimization and FEA analysis of Al-Si metal matrix composite drive shaft.* International Journal Of Engineering And Computer Science, 2014. **3**: p. 7713-7717.
14. Karthikeyan, M., R. Gupta, V. Rajesh, B. Ghosh, and P. Sinha, *Microstructural investigation on failure of internal drive shaft.* Journal of Failure Analysis and Prevention, 2007. **7**(6): p. 429-433.
15. Hueber, C., K. Horejsi, and R. Schledjewski, *Review of cost estimation: methods and models for aerospace composite manufacturing.* Advanced Manufacturing: Polymer & Composites Science, 2016. **2**(1): p. 1-13.

16. Bader, M.G., *Selection of composite materials and manufacturing routes for cost-effective performance.* Composites Part A: Applied science and manufacturing, 2002. **33**(7): p. 913-934.
17. Stott, P., *How climate change affects extreme weather events.* Science, 2016. **352**(6293): p. 1517-1518.
18. Hsiang, S.M. and A.S. Jina, *The causal effect of environmental catastrophe on long-run economic growth: Evidence from 6,700 cyclones*. 2014, National Bureau of Economic Research.
19. Klöpffer, W., *Background and future prospects in life cycle assessment*. 2014: Springer Science & Business Media.
20. La Rosa, A.D., G. Cozzo, A. Latteri, G. Mancini, A. Recca, and G. Cicala, *A comparative life cycle assessment of a composite component for automotive.* Chemical Engineering, 2013. **32**.
21. Witik, R.A., J. Payet, V. Michaud, C. Ludwig, and J.-A.E. Månson, *Assessing the life cycle costs and environmental performance of lightweight materials in automobile applications.* Composites Part A: Applied Science and Manufacturing, 2011. **42**(11): p. 1694-1709.
22. Kaw, A.K., *Mechanics of Composite Materials*. 2005: CRC Press.
23. Ashby, M.F. and D. CEBON, *Materials selection in mechanical design.* Le Journal de Physique IV, 1993. **3**(C7): p. C7-1-C7-9.
24. Rangaswamy, T., S. Vijayarangan, R. Chandrashekar, T. Venkatesh, and K. Anantharaman. *Optimal design and analysis of automotive composite drive shaft*. in *International Symposium of Research Students on Materials Science and Engineering December*. 2002.
25. Chang, K.-H., *Design theory and methods using CAD/CAE: The computer aided engineering design series*. 2014: Academic Press.
26. Mallick, P.K., *Fiber-reinforced composites: materials, manufacturing, and design*. 2007: CRC press.
27. Hill, C. and A. Norton, *LCA database of environmental impacts to inform material selection process.* DACOMAT project, Deliverable, 2018(6.1).
28. Shotton-Gale, N.E.H., *Clean filament winding: process optimisation (PhD thesis)*. 2013, University of Birmingham.
29. Jones, R.M., *Mechanics of Composite Materials, Taylor & Francis.* Inc., USA, 1999.
30. Qin, Y., J. Summerscales, J. Graham-Jones, M. Meng, and R. Pemberton, *Monomer selection for in situ polymerization infusion manufacture of natural-fiber reinforced thermoplastic-matrix marine composites.* Polymers, 2020. **12**(12): p. 2928.
31. Park, J.H. and S.C. Jana, *Mechanism of exfoliation of nanoclay particles in epoxy− clay nanocomposites.* Macromolecules, 2003. **36**(8): p. 2758-2768.
32. Pimenta, S. and S.T. Pinho, *Recycling carbon fibre reinforced polymers for structural applications: Technology review and market outlook.* Waste management, 2011. **31**(2): p. 378-392.
33. Dissanayake, N.P.J., *Life cycle assessment of flax fibres (PhD thesis)*. 2011, University of Plymouth.
34. Import-Export, L.B. *Basalt Fibers*. 2022; Available from: http://www.lbie.com/PDF/n3011.pdf.
35. Hancox, N.L., *Fibre composite hybrid materials*. 1981: Applied Science.
36. Inman, M., E.R. Thorhallsson, and K. Azrague, *A mechanical and environmental assessment and comparison of basalt fibre reinforced polymer*

(BFRP) rebar and steel rebar in concrete beams. Energy Procedia, 2017. **111**: p. 31-40.
37. Howarth, J., S.S. Mareddy, and P.T. Mativenga, *Energy intensity and environmental analysis of mechanical recycling of carbon fibre composite.* Journal of Cleaner Production, 2014. **81**: p. 46-50.
38. Tefera, G., G. Bright, and S. Adali, *Flexural and shear properties of CFRP laminates reinforced with functionalized multiwalled CNTs.* Nanocomposites, 2021. **7**(1): p. 141-153.
39. Mirsalehi, S.A., A.A. Youzbashi, and A. Sazgar, *Enhancement of out-of-plane mechanical properties of carbon fiber reinforced epoxy resin composite by incorporating the multi-walled carbon nanotubes.* SN Applied Sciences, 2021. **3**(6): p. 1-12.
40. Akcin, Y., S. Karakaya, and O. Soykasap, *Electrical, thermal and mechanical properties of CNT treated prepreg CFRP composites.* Materials Sciences and Applications, 2016. **7**(09): p. 465.
41. Dillard, D.A., *Advances in structural adhesive bonding*. 2010: Elsevier.
42. McCartney, L.N., *Predicting properties of undamaged and damaged carbon fibre reinforced composites*, in *The Structural Integrity of Carbon Fiber Composites*. 2017, Springer. p. 425-467.
43. Mengal, A.N., S. Karuppanan, and A.A. Wahab. *Basalt carbon hybrid composite for wind turbine rotor blades: a short review*. in *Advanced Materials Research*. 2014. Trans Tech Publ.
44. Wessexresins. *M1049/2048 technical data*. 2022 [cited 2022; Available from: https://wessexresins.co.uk/wp-content/uploads/sites/13/2020/10/PRO-SET-M1049-with-M2048-Medium-Cure-Bio-Based-Infusion-Epoxy-Rev-1.pdf.
45. Georgantzinos, S.K., P.A. Antoniou, G.I. Giannopoulos, A. Fatsis, and S.I. Markolefas, *Design of laminated composite plates with carbon nanotube inclusions against buckling: Waviness and agglomeration effects.* Nanomaterials, 2021. **11**(9): p. 2261.
46. Georgantzinos, S.K., P.A. Antoniou, and S.I. Markolefas, *A Multi-Scale Method for Designing Hybrid Fiber-Reinforced Composite Drive Shafts with Carbon Nanotube Inclusions.* Journal of Composites Science, 2021. **5**(6): p. 157.
47. Affdl, J.H. and J. Kardos, *The Halpin-Tsai equations: a review.* Polymer Engineering & Science, 1976. **16**(5): p. 344-352.
48. Flügge, W., *Statik und dynamik der schalen*. 2013: Springer-Verlag.
49. Sadowski, A.J. and J.M. Rotter, *Solid or shell finite elements to model thick cylindrical tubes and shells under global bending.* International Journal of Mechanical Sciences, 2013. **74**: p. 143-153.
50. Yeh, J. and I. Tadjbakhsh, *Stress singularity in composite laminates by finite element method.* Journal of composite materials, 1986. **20**(4): p. 347-364.
51. Lutz, G. and V. Getriebebau. *The Puck theory of failure in laminates in the context of the new guideline VDI 2014 Part 3*. in *Conference on damage in composite materials*. 2006.
52. Kelly, A. and C. Zweben, *Comprehensive composite materials.* Materials Today, 1999. **2**(1): p. 20-21.
53. Barbero, E.J., *Finite element analysis of composite materials using AbaqusTM*. Vol. 2103. 2013: CRC press Boca Raton.
54. Talreja, R., *On Failure Theories for Composite Materials*, in *Advanced Methods of Continuum Mechanics for Materials and Structures*. 2016, Springer. p. 379-388.

55. Puck, A. and H. Schürmann, *Failure analysis of FRP laminates by means of physically based phenomenological models*, in *Failure criteria in fibre-reinforced-polymer composites*. 2004, Elsevier. p. 832-876.
56. Ansys, *ANSYS reference manual*. 2022.
57. Tsai, S.W. and J.D.D. Melo, *An invariant-based theory of composites.* Composites Science and Technology, 2014. **100**: p. 237-243.
58. Tsai, S.W. and E.M. Wu, *A general theory of strength for anisotropic materials.* Journal of composite materials, 1971. **5**(1): p. 58-80.
59. Smith, C.B., *Some new types of orthotropic plates laminated of orthotropic material.* 1953.
60. Pister, K. and S. Dong, *Elastic bending of layered plates.* Journal of the Engineering Mechanics Division, 1959. **85**(4): p. 1-10.
61. Reissner, E. and Y. Stavsky, *Bending and stretching of certain types of heterogeneous aeolotropic elastic plates.* 1961.
62. Stavsky, Y., *On the general theory of heterogeneous aeolotropic plates.* Aeronautical Quarterly, 1964. **15**(1): p. 29-38.
63. Kollar, L.P. and G.S. Springer, *Mechanics of composite structures*. 2003: Cambridge university press.
64. Boiler, A., *ASME Boiler and Pressure Vessel Code: An International Code*. 1998: American Society of Mechanical Engineers New York.
65. Quaresimin, M., M. Ricotta, and L. Susmel. *Fatigue life prediction of composite laminates*. in *11th European conference on composite materials (ECCM-11), May 31eJune 3 2004 Rhodes, Greece*. 2004.
66. Geyer, R., *Parametric assessment of climate change impacts of automotive material substitution.* Environmental science & technology, 2008. **42**(18): p. 6973-6979.
67. Ansys, *Granta Edupack reference manual*. 2022.
68. Dahlben, L.J., M.J. Eckelman, A. Hakimian, S. Somu, and J.A. Isaacs, *Environmental life cycle assessment of a carbon nanotube-enabled semiconductor device.* Environmental science & technology, 2013. **47**(15): p. 8471-8478.
69. Tata-steel, *Sustainable Steel for Cars: Life-Cycle Carbon Footprint of a Front-End Module*. 2016.
70. Tapper, R.J., M.L. Longana, A. Norton, K.D. Potter, and I. Hamerton, *An evaluation of life cycle assessment and its application to the closed-loop recycling of carbon fibre reinforced polymers.* Composites Part B: Engineering, 2020. **184**: p. 107665.
71. Eberle, R. and H.A. Franze, *Modelling the use phase of passenger cars in LCI.* SAE transactions, 1998: p. 1998-2007.
72. Khan, A.M., N. He, L. Li, W. Zhao, and M. Jamil, *Analysis of productivity and machining efficiency in sustainable machining of titanium alloy.* Procedia Manufacturing, 2020. **43**: p. 111-118.
73. Asmatulu, E., J. Twomey, and M. Overcash, *Recycling of fiber-reinforced composites and direct structural composite recycling concept.* Journal of Composite Materials, 2014. **48**(5): p. 593-608.
74. Mahltig, B. and Y. Kyosev, *Inorganic and composite fibers: production, properties, and applications*. 2018: Woodhead Publishing.
75. Nowack, B., R.M. David, H. Fissan, H. Morris, J.A. Shatkin, M. Stintz, R. Zepp, and D. Brouwer, *Potential release scenarios for carbon nanotubes used in composites.* Environment international, 2013. **59**: p. 1-11.

76. Ashby, M.F. and D. Cebon, *Materials selection in mechanical design.* MRS Bull, 2005. **30**(12): p. 995.
77. Stewart, R., *Filament winding spins light, strong composite structures with precision.* Reinforced Plastics, 2009. **53**(5): p. 34-39.
78. Summerscales, J., N.P. Dissanayake, A.S. Virk, and W. Hall, *A review of bast fibres and their composites. Part 1–Fibres as reinforcements.* Composites Part A: Applied Science and Manufacturing, 2010. **41**(10): p. 1329-1335.
79. Byrne, N., R. De Silva, Y. Ma, H. Sixta, and M. Hummel, *Enhanced stabilization of cellulose-lignin hybrid filaments for carbon fiber production.* Cellulose, 2018. **25**(1): p. 723-733.
80. Eichhorn, S.J., A. Dufresne, M. Aranguren, N. Marcovich, J. Capadona, S.J. Rowan, C. Weder, W. Thielemans, M. Roman, and S. Renneckar, *Current international research into cellulose nanofibres and nanocomposites.* Journal of materials science, 2010. **45**(1): p. 1-33.
81. Gutiérrez, E. and F. Bono, *Review of industrial manufacturing capacity for fibre-reinforced polymers as prospective structural components in shipping containers.* JRC Scientific and Policy Reports, JRC77823, 2013.
82. Douglas, A., R. Carter, M. Li, and C.L. Pint, *Toward small-diameter carbon nanotubes synthesized from captured carbon dioxide: critical role of catalyst coarsening.* ACS applied materials & interfaces, 2018. **10**(22): p. 19010-19018.
83. Cushman-Roisin, B. and B.T. Cremonini, *Data, Statistics, and Useful Numbers for Environmental Sustainability: Bringing the Numbers to Life*. 2021: Elsevier.
84. Gutowski, T.G., J.Y. Liow, and D.P. Sekulic. *Minimum exergy requirements for the manufacturing of carbon nanotubes*. in *Proceedings of the 2010 IEEE international symposium on sustainable systems and technology*. 2010. IEEE.
85. Matanza, A., G. Vargas, I. Leon, M. Pousse, N. Salmon, and C. Marieta, *Life cycle analysis of standard and high-performance cements based on carbon nanotubes composites for construction applications.* World SB, 2014. **4**: p. 28-30.
86. Ross, A. *Basalt fibers: alternative to glass?* CompositesWorld 2006; Available from: https://www.compositesworld.com/articles/basalt-fibers-alternative-to-glass.

Appendix A – Decision Matrix Data

Table A-A1. Manufacturing Decision Matrix Data

Property	Unit	RIFT		HLU		PrePreg		RTM		Filament winding	
Fibre volume fraction (VF)	%	40-60	[26]	20-50	[26]	50-70	[26]	20-60	[26]	50-70	[28]
Max Size (Length)	m	>100	[26]	>100	[26]	20	[26]	20	[26]	60	[77]
Cycle Time	hr	5-1400	[26]	5-1400	[26]	2.0-10	[26]	1-20.0	[26]	1-20.0	[26]
Material cost (5 High)	NA	3	Estimate	2	[26]	5	[26]	3	[26]	3	Estimate
Tool cost (5 High)	NA	1	Estimate	1	[26]	3	[26]	4	[26]	3	Estimate
Labour cost (5 High)	NA	4	Estimate	4	[26]	4	[26]	3	[26]	2	Estimate
Labour skill rating (5 High)	NA	4	Estimate	2	[26]	4	[26]	3	[26]	2	Estimate
Quality	NA	4	Estimate	2	[26]	5	[26]	4	[26]	2	Estimate
Embodied energy	MJ/kg	41	[27]	77	[27]	160	[27]	51	[27]	11	[27]
Environmental hazard (1 Bad)	NA	3	Estimate	1	[26]	5	[26]	3	[26]	4	Estimate

Table A-A2. Manufacturing Decision Matrix Weighting

Factors	weighting 1-5	RIFT		HLU		PrePreg		RTM		Filament winding	
		Score	Weighted Score	Score	Weighted Score	Score	Weighted Score	Score	Weighted Score	Score	Weighted Score
VF	5	4	20	2	10	5	25	3	15	5	25
Max Size (Length)	2	5	10	5	10	3	6	3	6	4	8
Cycle Time	4	3	12	3	12	5	20	5	20	2	8
Material cost (5 High)	2	3	6	2	4	5	10	3	6	3	6
Tool cost (5 High)	3	5	15	5	15	5	15	2	6	3	9
Labour cost (5 High)	4	2	8	2	8	2	8	3	12	4	16
Quality	2	4	8	2	4	5	10	4	8	2	4
Embodied energy	3	4	12	2	6	1	3	4	12	5	15
Environmental hazard	4	4	16	1	4	5	20	4	16	2	8
SUM			107		73		117		101		99

Volume fraction was given the highest weighting as it contributes significantly to composites properties. Size was given a low weighting as the drive shaft is small in comparison to part typically manufactured from composites for the aerospace industry. Material cost was given a low weighting as some process require specific materials which can contribute significantly to the cost of the final product the benefits typically outweigh the costs. Tool cost was given a medium weighting as while tool costs can be high these can be considered over medium to long production runs. Labour costs were given a high weighting as the can be contributed to each part. Quality was given a low weighting as while the products quality can effect its performance, customers are unlikely to directly perceive the drive shaft unless it fails. Embodied energy was given a medium rating as a high energy process will results in the part with high embodied energy and hence carbon footprint. Environmental hazard was given a high rating as the composite production can have detrimental effects on both the environment and workers.

Table A-B1. Matrix Decision Matrix Weighting

Factors	weighting 1-5	Epoxy		Polyester		PA6		PMMA (Elium)		Bio Epoxy		Bio Polyester		Recycled Polyester	
		Score	Weighted Score	Score	Weighted Score	Score	Weighted Score	Score	Weighted Score	Score	Weighted Score	Score	Weighted Score	Score	Weighted Score
Density	5	4	20	3	15	5	25	4	20	5	25	3	15	4	20
Cost	3	4	12	5	15	5	15	1	3	2	6	3	9	2	6
Tensile modulus	4	5	20	4	16	3	12	3	12	3	12	3	12	3	12
Tensile Strength	3	4	12	3	9	3	9	2	6	4	12	4	12	5	15
Processing temperature	5	5	25	5	25	0	0	4	20	5	25	5	25	5	25
Reusable/Recyclable	3	0	0	0	0	5	15	5	15	0	0	0	0	0	0
Renewable resource	2	0	0	0	0	5	10	3	6	5	10	5	10	5	10
SUM			89		80		86		82		90		83		88

Density was set with the highest weighting as reducing weight is a key reason for using composites. Cost was given a middle/low weighting as it was assumed customers/manufactures would be willing to associate the high cost associated with carbon fibre/composites. Modulus was given a high weighting as shaft thickness and material modulus are proportional. Strength was given a low/medium weighting as the matrix contributes little strength to the composite. Processing temperature was given a high weighting as all matrixes must be processable at room temperature for the chosen manufacturing method. Recyclability was given a low/medium weighting as while the matrix plays a role in the ease of recycling for composites. Renewable resource was given a low weighting as while sustainability is key to customers performance is still preferable for most customers.

Table A-B2. Matrix Decision Matrix Data

Property	Unit	Epoxy		Polyester		PA6		PMMA (Elium)		Bio Epoxy	
Density	g/cm^3	1.1-1.4	[29]	1.2-1.5	[29]	1.13	[30]	1.2	[30]	1.16	[31]
Cost	£/kg	1.5-12	[29]	0.9-1.5	[29]	1.3-1.5	[30]	ND(High)	[30]	16	[31]
Tensile modulus	GPa	3.0-6.0	[29]	2-4.5	[29]	2-3.8	[30]	2-3.8	[30]	1.35-3.2	[31]
Tensile Strength	MPa	35-100	[29]	40-90	[29]	85	[30]	66	[30]	30-110	[31]
Recyclable		No	Ts	No	Ts	yes	Tp	Yes	Tp	No	Tp
Processing temperature		RT	[26]	RT	[26]	130-200	[30]	20-100	[30]	RT	[31]
Renewable source		No		No		Yes	[30]	Possible	[30]	Up to 60%	[31]

Table A-C1. Fibre Decision Matrix Data 1

Property	Unit	Recycled Carbon Fibre		Natural Fibre		Cellulose Carbon Fibre	
Density	g/cm^3	1.8-2	[32]	1.2-1.5	[78]	1.4-1.5	[79, 80]
Tensile Modulus	GPa	205-240	[32]	5-130	[78]	40-230	[79, 80]
Tensile Strength	GPa	3.1-5.1	[32]	0.01-1.8	[78]	0.9-2.2	[79, 80]
Embodied Energy	MJ/kg	10.8-36	[33]	59-86	[30]	ND(high)	
Max Operating Temperature		500	[34]	150-200	[30]	ND	
Renewable source	Y/N	No		Yes	[30]	Yes	[79, 80]

Table A-C2. Fibre Decision Matrix Data 2

Property	Unit	Carbon Fibre		Aramid		Basalt		Glass Fibre	
Density	g/cm^3	1.8-2.0	[26]	1.4	[26]	2.63-2.8	[34]	2.5-2.6	[35]
Tensile Modulus	GPa	200-400	[26]	120	[26]	90-110	[34]	70-90	[35]
Tensile Strength	GPa	3.2-5.4	[26]	2.8	[26]	4.1-4.8	[34]	3.4-4.6	[35]
Embodied Energy	MJ/kg	183-236	[37]	135-1700	[56]	18	[36]	13-32	[37]
Max Operating Temperature		500	[34]	250	[34]	650	[34]	300-380	[34]
Renewable source	Y/N	No		No		Yes		No	

Table A-C3. Fibre Decision Matrix Weighting 2

Factors	weighting 1-5	CF		Aramid		Basalt		Glass Fibre	
		Score	Weighted Score	Score	Weighted Score	Score	Weighted Score	Score	Weighted Score
Density	5	4	20	5	25	2.5	12.5	3	15
Flexural Modulus	4	5	20	4	16	4	16	3.5	14
Flexural Strength	3	5	15	3	9	5	15	4	12
Embodied energy	2	1	2	1	2	5	10	4	8
Max operating temperature	1	4	4	2	2	5	5	3	3
Renewable resource	2	0	0	0	0	3	6	0	0
SUM			61		54		64.5		52

Density was set with the highest weighting as reducing weight is a key reason for using composites. Cost was given a middle/low weighting as it was assumed customers/manufactures would be willing to associate the high cost associated with carbon fibre/composites. Modulus was given a high weighting as shaft thickness and material modulus are proportional. Strength was given a low/medium weighting as composites are typically used for their stiffness rather than strength. Embodied energy was given a medium rating as parts with a high embodied energy typically have a large carbon footprint. Processing temperature was given a high weighting as all matrixes must be processable at room temperature for the chosen manufacturing method. Recyclability was given a low/medium weighting as while the matrix plays a role in the ease of recycling for composites. Renewable resource was given a low weighting as while sustainability is key to customers performance is still preferable for most customers.

Table A-C. Fibre Decision Matrix Weighting 1

Factors	**weighting 1-5**	**Recycled CF**		**NF**		**Cellulose CF**	
		Score	Weighted Score	Score	Weighted Score	Score	Weighted Score
Density	5	4	20	5	25	5	25
Flexural Modulus	4	2	8	2.5	10	3	12
Flexural Strength	3	2	6	1	3	2	6
Embodied energy	2	3	6	2	4	0	0
Max operating temperature	1	4	4	2	2		0
Renewable resource	2	0	0	5	10	5	10
SUM			44		54		53

Appendix B – Life Cycle Inventory Data

Table B1. Life Cycle Inventory Data - Production Cost

Steel	Production						
	Definition				Pricing		
	Name	Amount	Unit	Source	£/kg	Source	Cost
	Steel Production	4.9	kg	Shaft Mass	0.737	[56]	3.6
	Totals						3.6
Carbon	Production						
	Definition				Pricing		
	Name	Amount	Unit	Source	£/kg	Source	Cost
	Carbon/Epoxy Prepreg Production	0.44	kg	Shaft Mass	32	[56]	13.9
	Shaft Production (Filament Winding)	0.44	kg	Shaft Mass	5.28	[81]	2.3
	Totals						16.2
Basalt	Production						
	Definition				Pricing		
	Name	Amount	Unit	Source	£/kg	Source	Cost
	Basalt/Epoxy Prepreg Production	1.33	kg	Shaft Mass	16.50	Supplementary Data	21.9
	Shaft Production (Filament Winding)	1.33	kg	Shaft Mass	5.28	[81]	7.0
	Totals						29.0
Nano	Production						
	Definition				Pricing		
	Name	Amount	Unit	Source	£/kg	Source	Cost
	Carbon/Nano/Epoxy Prepreg Production	0.42	kg	Shaft Mass	182	[82]	77.1
	Shaft Production (Filament Winding)	0.42	kg	Shaft Mass	5.28	[81]	2.2
	Totals						79.3

Table B2. Life Cycle Production Inventory Data Embodied Energy and CO2 per kg

	Production					
Steel	Inputs			Outputs		
	MJ/kg	Source	MJ	CO2 kg/kg	Source	CO2 (kg)
	20.5	[56]	100.5	1.55	[56]	7.6
			100.5			7.6
	Production					
Carbon	Inputs			Outputs		
	MJ/kg	Source	MJ	CO2 kg/kg	Source	CO2 (kg)
	750	[56]	326.8	50	[56]	21.8
	2.7	[83]	1.2	1.84	[83]	0.8
			328.0			22.6
	Production					
Basalt	Inputs			Outputs		
	MJ/kg	Source	MJ	CO2 kg/kg	Source	CO2 (kg)
	438.36	Supplementary Data	583.0	31.54	Supplementary Data	41.9
	2.7	[83]	3.6	1.84	[83]	2.4
			403.4			31.0
	Production					
CNT	Inputs			Outputs		
	MJ/kg	Source	MJ	CO2 kg/kg	Source	CO2 (kg)
	320450	[84]	135679.1	799	[85]	338.3
	2.7	[83]	1.1	1.84	[83]	0.8
			1.36E+05			339.1

Table B3. Supplementary Data

Impact of Basalt Epoxy Composite					
Category	Item	Symbol	Value	Formula	Source
Cost	Cost of Basalt Fibre (£/kg)	Bf-C	5.00		[86]
	Cost of Bio-Epoxy (£/kg)	Be-C	6.00		[44]
	Assumed Cost of Pre-Preg	Bepp-C	16.50	(Cbf+Cbe)*1.5	
Energy	Basalt Fibre (MJ/kg)	Bf-EE	0.96		[36]
	Carbon Fibre (MJ/kg)	Cf-EE	300.00		[56]
	Epoxy Resin (MJ/kg)	E	126.00		[56]
	Bio-Epoxy Resin (MJ/kg)	Be	113.40	E*0.9	
	Carbon Fibre Pre-Preg (MJ/kg)	Cfpp-EE	750.00		[56]
	Basalt Fibre Pre-Preg (MJ/kg)	Bepp-EE	438.36	Cfpp-(Cf-Bf)-(e-Be)	
CO2	Basalt Fibre (kg/kg)	Bf-CO2	0.06		[36]
	Carbon Fibre (kg/kg)	Cf-CO2	21.30		[56]
	Epoxy Resin (kg/kg)	E	6.23		
	Bio-Epoxy Resin (kg/kg)	Be	5.61	e*0.9	[56]
	Carbon Fibre Pre-Preg (kg/kg)	Cfpp-CO2	53.40		[56]
	Basalt Fibre Pre-Preg (kg/kg)	Bepp-CO2	31.54	Cfpp-(Cf-Bf)-(e-Be)	

Table B4. Life Cycle Use Phases Inventory Data CO2 Savings

Steel	Use				
	Fuel Savings				
	Name	Weight Saving	CO2 Savings kg CO2/kg	CO2 Savings (kg)	Source
	Lifetime saving CO2	0.00	-6	0	(Geyer, 2008)
	Totals			0	
Carbon	Use				
	Fuel Savings				
	Name	Weight Saving	CO2 Savings kg CO2/kg	CO2 Savings (kg)	Source
	Lifetime saving CO2	4.46	-6	-26.8	(Geyer, 2008)
	Totals			-26.8	
Basalt	Use				
	Fuel Savings				
	Name	Weight Saving	CO2 Savings kg CO2/kg	CO2 Savings (kg)	Source
	Lifetime saving CO2	3.57	-6	-21.4	(Geyer, 2008)
	Totals			-21.4	
Nano	Use				
	Fuel Savings				
	Name	Weight Saving	CO2 Savings kg CO2/kg	CO2 Savings (kg)	Source
	Lifetime saving CO2	4.48	-6	-26.9	(Geyer, 2008)
	Totals			-26.9	

Table B5. Life Cycle Disposal Inventory Data Price

Steel	Disposal							
	Definition					Pricing		
	Name	Amount	Unit	Source	£/kg	Source	Cost	
	Recycling	4.90	kg	Shaf Mass	43	(WRAP, 2020)	210.7	
	Totals						210.7	
Carbon	Disposal							
	Definition					Pricing		
	Name	Amount	Unit	Source	£/kg	Source	Cost	
	Carbon/Epoxy Disposal (incineration)	0.44	kg	Shaf Mass	95	(WRAP, 2020)	41.4	
	Totals						41.4	
Basalt	Disposal							
	Definition					Pricing		
	Name	Amount	Unit	Source	£/kg	Source	Cost	
	Basalt/Epoxy Disposal (incineration)	1.33	kg	Shaf Mass	95	(WRAP, 2020)	126.3	
	Totals						126.3	
Nano	Disposal							
	Definition					Pricing		
	Name	Amount	Unit	Source	£/kg	Source	Cost	
	Carbon/Epoxy Disposal (incineration)	0.42	kg	Shaf Mass	95	(WRAP, 2020)	40.2	
	Totals						40.2	

Table B6. Life Cycle Disposal Inventory Data Energy and Carbon Emissions

Steel	Disposal								
	Definition			Inputs			Outputs		
	Name	Amount	Unit	MJ/kg	Source	MJ	CO2 kg/kg	Source	CO2 (kg)
	Recycling	4.90	kg	8.96	(ANSYS, 2021)	43.904	0.70	Edupack	3.4
	Totals					43.9			3.4
Carbon	Disposal								
	Definition			Inputs			Outputs		
	Name	Amount	Unit	MJ/kg	Source	MJ	CO2 kg/kg	Source	CO2 (kg)
	Carbon/Epoxy Disposal (incineration)	326.81	kg	-32.9	(ANSYS, 2021)	-14.3	3.33	(ANSYS, 2021)	1.5
	Totals					-14.3			1.5
Basalt	Disposal								
	Definition			Inputs			Outputs		
	Name	Amount	Unit	MJ/kg	Source	MJ	CO2 kg/kg	Source	CO2 (kg)
	Basalt/Epoxy Disposal (incineration)	399.81	kg	-32.9	(ANSYS, 2021)	-43.8	3.33	(ANSYS, 2021)	4.4
	Totals					-43.8			4.4
Nano	Disposal								
	Definition			Inputs			Outputs		
	Name	Amount	Unit	MJ/kg	Source	MJ	CO2 kg/kg	Source	CO2 (kg)
	Carbon/Epoxy Disposal (incineration)	135679.12	kg	-32.9	(ANSYS, 2021)	-13.9	3.33	(ANSYS, 2021)	1.4
	Totals					-13.9			1.4